Available online at www.sciencedirect.com

ScienceDirect

Nuclear Physics B 971 (2021) 115524

NUCLEAR PHYSICS B

www.elsevier.com/locate/nuclphysb

Distinguishing Leptoquarks at the LHC/FCC

Priyotosh Bandyopadhyay [a], Saunak Dutta [a,*], Mahesh Jakkapu [b], Anirban Karan [a,*]

[a] *Indian Institute of Technology Hyderabad, Kandi, Sangareddy-502285, Telengana, India*
[b] *Graduate University for Advanced Studies (SOKENDAI), Shonan Village, Hayama, Kanagawa 240-0193, Japan*

Received 5 April 2021; received in revised form 3 August 2021; accepted 21 August 2021
Available online 24 August 2021
Editor: Hong-Jian He

Abstract

In this article, we deal with how to distinguish the signatures of different Leptoquarks at the LHC/FCC if all of them lie within similar mass and coupling range and can be produced at present and future colliders. It has been found that hard scattering cross-sections and angular distributions can be used to differentiate scalar and vector Leptoquarks. On the other hand, final state topology and determination of jet charge can separate Leptoquarks with same spin even from same $SU(2)_L$ multiplet. We performed a PYTHIA8 based analysis considering all the dominant Standard Model (SM) backgrounds at the LHC/FCC with centre of mass energies of 14, 27 and 100 TeV for scalar (S_1) and vector ($\widetilde{U}_{1\mu}$) Leptoquarks. We see that confirming evidence of scalar Leptoquark at 14 TeV requires 1000 fb^{-1} of integrated luminosity, whereas the vector Leptoquark can be probed with very early data. But, at 100 TeV with 1000 fb^{-1} of integrated luminosity, scalar Leptoquark of mass 3.5 TeV and vector Leptoquark of mass more than 5 TeV can be probed easily.

Contents

* Corresponding authors.
E-mail addresses: bpriyo@phy.iith.ac.in (P. Bandyopadhyay), ph17resch11002@iith.ac.in (S. Dutta), maheshj@post.kek.jp (M. Jakkapu), kanirban@iith.ac.in (A. Karan).

https://doi.org/10.1016/j.nuclphysb.2021.115524

1. Introduction

Leptoquarks are special kind of beyond Standard Model (BSM) particles carrying both non-zero lepton and baryon numbers [1–3]. Therefore, they can interact with quarks and leptons simultaneously. They are colour triplet (fundamental or anti-fundamental) as well as electromagnetically charged. However, under $SU(2)_L$ gauge representation, they could be singlet, doublet or triplet. Moreover, according to Lorentz transformation, they might be scalar (spin 0) and vector (spin 1) as well. The notion of Leptoquark has been there in literature for more than forty years. They appear naturally in various BSM scenarios involving higher gauge representations that unify the matter fields [4–13]. They are also quite useful in explaining various experimental and theoretical anomalies [14–37]. Their signatures at different colliders have been also studied widely for several phenomenological interests [38–71,75–86]. However, no conclusive evidence for their existence has been found yet.

In this paper, we investigate how to differentiate the signatures of scalar and vector Leptoquarks at the LHC/FCC. For this, we have to first assume that both type of Leptoquarks exists in nature with such masses and couplings that they can be produced at present and future colliders like LHC/FCC. In a PYTHIA8 [102] based analysis, we have looked into hard scattering cross-section, angular distribution, jet charge determination, transverse momenta of jet and lepton and few other aspects for this distinction. It turns out that total cross-section and angular distribution can be used to separate scalar and vector Leptoquarks at the LHC/FCC, whereas final state topology and determination of jet charge become instrumental in distinguishing Leptoquarks with same spin as well as Leptoquarks belonging to same $SU(2)_L$ multiplet.

A detailed PYTHIA8 [102] based simulation with all dominant SM backgrounds have been carried out which shows that the events number for vector Leptoquark could be a few times larger than the scalar one for the same choices of mass of Leptoquarks viz. $\widetilde{U}_{1\mu}$ and S_1. This attributes to the fact of more spin degrees of freedom for the former one and also due to higher branching for the allowed benchmark points. Reconstruction of Leptoquark mass along with the angular distribution in the centre of mass (CM) frame enable us to distinguish the spin representations

Table 1
Specification of scalar and vector Leptoquarks. The S_3^{adj} and $U_{3\mu}^{adj}$ are the scalar and vector triplet Leptoquarks in adjoint representation.

ϕ	$SU(3)$	Y_ϕ	T_3	Q_ϕ	Interaction (+ h.c.)
Scalar Leptoquarks $\boldsymbol{\phi_s}$					
S_1	$\overline{3}$	2/3	0	1/3	$Y_L\,\overline{\boldsymbol{Q}}_L^c\left(i\sigma^2 S_1\right)\boldsymbol{L}_L$ $+Y_R\,\overline{u}_R^c\,S_1\,\ell_R$
$\widetilde{S}_1$	$\overline{3}$	8/3	0	4/3	$Y_R\,\overline{d}_R^c\,\widetilde{S}_1\,\ell_R$
R_2	3	7/3	1/2 −1/2	5/3 2/3	$Y_L\,\overline{u}_R\left(i\sigma^2 R_2\right)^T\boldsymbol{L}_L$ $+Y_R\,\overline{\boldsymbol{Q}}_L\,R_2\,\ell_R$
$\widetilde{R}_2$	3	1/3	1/2 −1/2	2/3 −1/3	$Y_L\,\overline{d}_R\left(i\sigma^2\widetilde{R}_2\right)^T\boldsymbol{L}_L$
$\vec{S}_3$	$\overline{3}$	2/3	1 0 −1	4/3 1/3 −2/3	$Y_L\,\overline{\boldsymbol{Q}}_L^c\left(i\sigma^2 S_3^{adj}\right)\boldsymbol{L}_L$
Vector Leptoquarks $\boldsymbol{\phi_v}$					
$U_{1\mu}$	3	4/3	0	2/3	$Y_L\,\overline{\boldsymbol{Q}}_L\gamma^\mu\,U_{1\mu}\boldsymbol{L}_L$ $+Y_R\,\overline{d}_R\gamma^\mu\,U_{1\mu}\ell_R$
$\widetilde{U}_{1\mu}$	3	10/3	0	5/3	$Y_R\,\overline{u}_R\,\gamma^\mu\,\widetilde{U}_{1\mu}\,\ell_R$
$V_{2\mu}$	$\overline{3}$	5/3	1/2 −1/2	4/3 1/3	$Y_L\,\overline{d}_R^c\,\gamma^\mu\left(i\sigma^2 V_{2\mu}\right)^T\boldsymbol{L}_L$ $+Y_R\,\overline{\boldsymbol{Q}}_L^c\,\gamma^\mu\left(i\sigma^2 V_{2\mu}\right)\ell_R$
$\widetilde{V}_{2\mu}$	$\overline{3}$	−1/3	1/2 −1/2	1/3 −2/3	$Y_L\,\overline{u}_R^c\,\gamma^\mu\left(i\sigma^2\widetilde{V}_{2\mu}\right)^T\boldsymbol{L}_L$
$\vec{U}_{3\mu}$	3	4/3	1 0 −1	5/3 2/3 −1/3	$Y_L\,\overline{\boldsymbol{Q}}_L\,\gamma^\mu\,U_{3\mu}^{adj}\,\boldsymbol{L}_L$

of such Leptoquarks. We also comment on the possibility of obtaining different final states from a Leptoquarks in higher gauge representation. Their decays can be explored by the study of different final state topologies as well as the construction of the jet charges coming from the Leptoquark decays.

The paper is organised in the following way. We briefly describe all the scalar and vector Leptoquarks in the next section (Section 2). Section 3 deals with current experimental bounds on the masses and couplings of Leptoquarks and choice of benchmark points for simulation. The theoretical aspects for pair production of scalar and vector Leptoquarks at proton-proton collider have been illustrated in Section 4. In Section 5, we have discussed how to identify the signatures of scalar and vector Leptoquarks as well as the same of different excitations lying in the same $SU(2)_L$ multiplet. Finally, we conclude our study in Section 6.

2. Scalar and vector Leptoquarks

In this section, we discuss different scalar and vector Leptoquarks, their nomenclature and quantum numbers and interaction terms in brief. We have generically denoted the Leptoquarks

as $\phi_{s,v}$ indicating the scalar and vector types respectively. In Table 1, we summarize all the scalar and vector Leptoquarks. We follow the similar notations of Refs. [1,3,69–72] for the nomenclature of the Leptoquarks. The vector ones are indicated by the Lorentz index μ in the subscript of their names. Additionally, the subscripts 1, 2 and 3 in the names of Leptoquarks signify singlet, doublet and triplet Leptoquarks under $SU(2)_L$ gauge group. Thus we have five scalar (S_1 , $\widetilde{S}_1$, R_2 , $\widetilde{R}_2$ and $\vec{S}_3$) and five vector ($U_{1\mu}$, $\widetilde{U}_{1\mu}$, $V_{2\mu}$, $\widetilde{V}_{2\mu}$ and $\vec{U}_{3\mu}$) Leptoquarks and in each set there are two singlets, two doublets and one triplet. Different quantum numbers like $SU(3)$ behaviour, weak hypercharge (Y_ϕ), the third component of weak isospin (T_3), electromagnetic charge (Q_ϕ) as well as their interactions with quarks and leptons are also mentioned in Table 1. Here, $\boldsymbol{Q}_L$ and $\boldsymbol{L}_L$ are $SU(2)_L$ doublets for quarks and leptons given by $\boldsymbol{Q}_L = (u_L, d_L)^T$ and $\boldsymbol{L}_L = (\nu_L, l_L)^T$ respectively, whereas u_R, d_R and l_R represent all the three generations of right-handed $SU(2)_L$ singlets for up type quark, down type quark and charged lepton, respectively (the generation and colour indices are suppressed). The superscript "c" in the interaction terms indicates charge conjugate of a field. It is interesting to notice that for scalar Leptoquarks, only the doublets (R_2 and $\widetilde{R}_2$) are in fundamental representation of $SU(3)$ and the rest are in anti-fundamental representation whereas the scenario becomes reverse for vector Leptoquarks.

3. Experimental bounds and benchmark points

Before we choose benchmark points for collider simulation let us first summarize various bounds on the parameter-space of Leptoquarks. Several direct and indirect constraints on the masses and couplings of Leptoquarks have been studied in literature from different perspectives. Results from low energy experiments help to restrict the Leptoquark-induced four-fermion interactions which provide indirect bound on the parameter-space of the Leptoquarks. Refs. [32,36,72–74] deal with the indirect constraints on Leptoquarks in a quite extensive manner. All the indirect bounds on Leptoquarks are listed in the "Indirect Limits for Leptoquarks" section of Ref. [2]. However, we mainly focus on the direct bounds on Leptoquarks coming from the chance for them to be detected at various high energy colliders.

The experimental hunt for Leptoquarks started around thirty five years ago. The CELLO [87] and JADE [88] Collaborations were the first to search for Leptoquarks at the PETRA through their pair production in e^+e^- collision. After that the AMY Collaboration [89] at TRISTAN, the ALEPH [90], L3 [91], OPAL [92] and DELPHI [55] Collaborations at LEP, the H1 [95] and ZEUS [93,94] Collaborations at HERA, the UA2 Collaboration [57] at CERN, the CDF [96–98] and DØ [99–101] Collaborations at Fermilab Tevatron have done exhaustive work to get the first evidence of Leptoquark. But none of them succeeded in discovering Leptoquark and thus the direct bound on the parameter-space of Leptoquarks arise. After each experiment the allowed mass for Leptoquark gets higher than the previous analysis.

The strongest constraints till now on Leptoquarks come from the ATLAS and CMS Collaborations at the LHC. The ATLAS Collaboration has looked for pair production of first and second generation Leptoquarks with the $\mathcal{L}_{int} = 36.1$ fb^{-1} data set of the LHC at $\sqrt{s} = 13$ TeV. However, they cannot find any conspicuous signal over SM background, and hence they rule out first and second generation of scalar Leptoquarks with masses below 1400 GeV (1290 GeV) and 1560 GeV (1230 GeV) at 95% C.L. assuming branching $\beta = 1\,(0.5)$ [63]. Using same data set they have also excluded third generation scalar Leptoquark lighter than 800 GeV irrespective of any branching fraction [62]. The CMS Collaboration has also performed similar analysis taking the LHC data set at $\mathcal{L}_{int} = 35.9$ fb^{-1} and $\sqrt{s} = 13$ TeV. They put lower bounds on the masses of first and second generation scalar Leptoquarks to be 1435 GeV (1270 GeV) and 1530 GeV

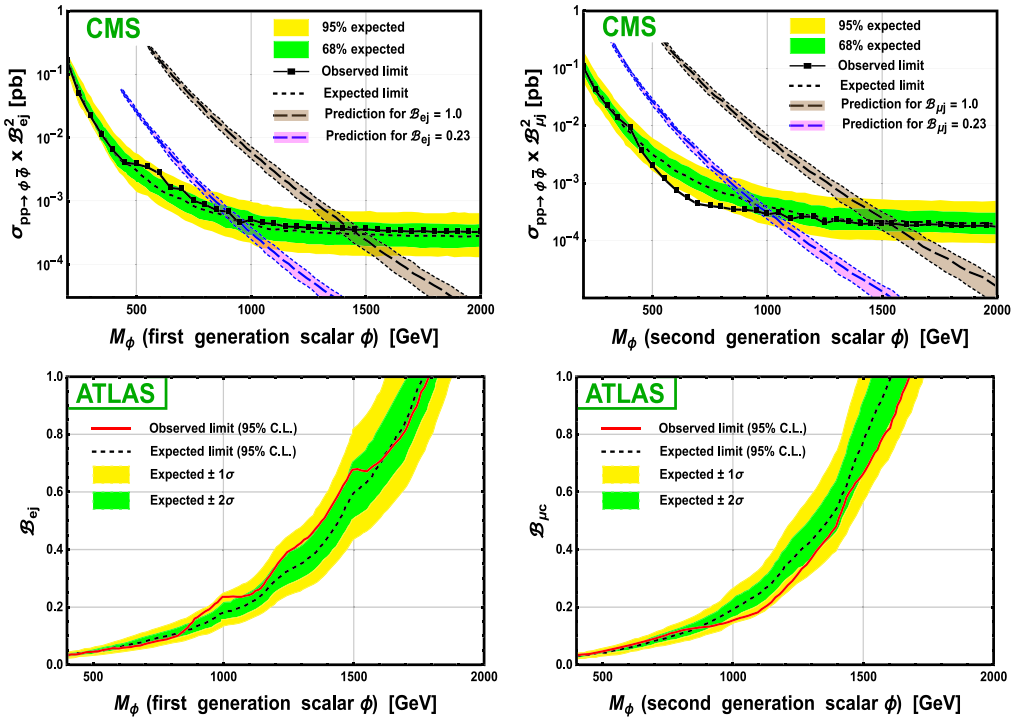

Fig. 1a. LHC bounds on first and second generations of scalar Leptoquarks. First and second plots show the constraints from CMS on $\sigma_{pp\to\phi\bar{\phi}} \times \mathcal{B}^2$ for first and second generations of scalar Leptoquarks decaying to a jet and charged lepton [64,65]. Third and fourth plots illustrate the bounds from ATLAS on the branching fractions of the same Leptoquarks to a jet and electron or c-jet and muon [110]. The black dotted lines indicate the expected limits whereas the black solid lines with small squares (or the solid red lines) depict the observed limits. The green and yellow bands describe the 1σ and 2σ regions respectively over the expected limits. The black and blue dashed curve (along with brown and magenta shades on them) signify the theoretical prediction for the pair production of Leptoquarks (with theoretical uncertainties) with branching 100% and 23% respectively to a particular mode. (For interpretation of the colours in the figure(s), the reader is referred to the web version of this article.)

(1285 GeV) respectively for $\beta = 1$ (0.5) at 95% C.L. [64,65]. About third generation scalar Leptoquarks, CMS Collaboration has reported at 95% C.L. that they should be heavier than 900 GeV and 1020 GeV, if they decay to top-quark plus τ-lepton and bottom-quark plus τ-lepton respectively with $\beta = 1$ [66,67]. On the other hand, bounds on vector Leptoquarks have been drawn from neutrino decay channels only. Results from CMS Collaboration [68] states that if a vector Leptoquark decays to $t\nu$ and $b\tau$ channels with 50% branching fractions in each, then it should have mass larger than 1530 GeV (1115 GeV) is excluded for $\kappa = 1$ ($\kappa = 0$). At this point, it is worth mentioning that $\kappa (\equiv 1 - \kappa_G)$ is a dimensionless parameter related to the *anomalous chromo-magnetic moment* and *anomalous chromo-electric dipole moment* of the vector Leptoquarks. The interactions of gluons with vector Leptoquarks depend on this parameter [54]. The case with $\kappa = 1$ is usually termed as *Yang-Mills* coupling whereas the scenario with $\kappa = 0$ is called *minimal* coupling. In Figs. 1a, 1b and 1c we have illustrated all the current bounds on scalar and vector Leptoquarks. While Fig. 1a shows ATLAS and CMS bounds on first and second generations of scalar Leptoquarks, Fig. 1b indicates the same on third generation scalar Lepto-

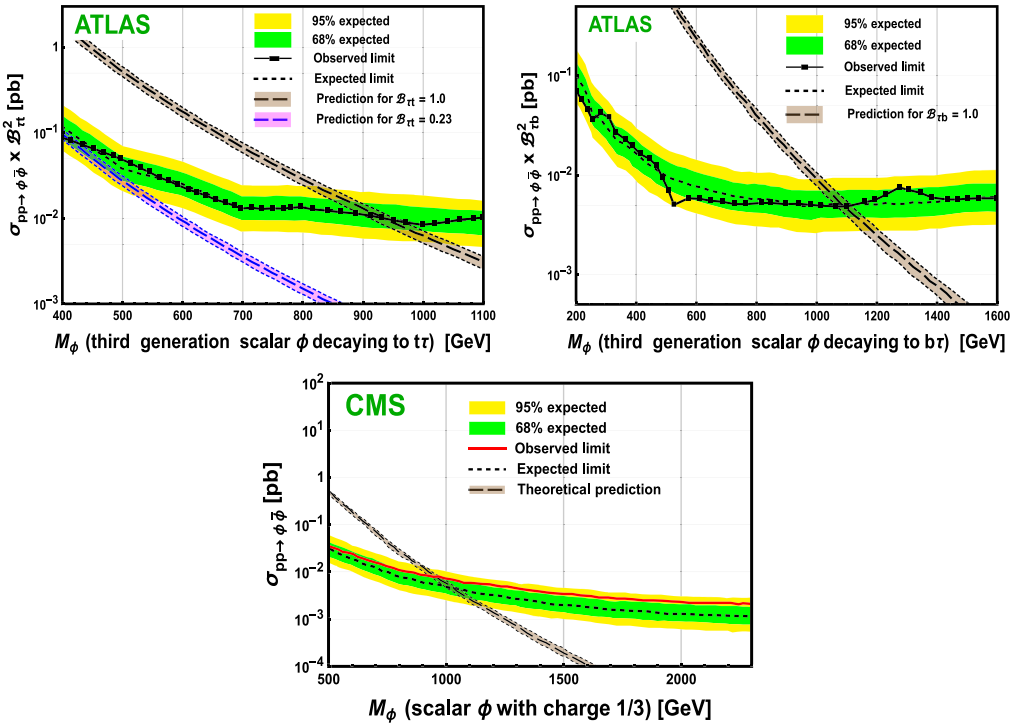

Fig. 1b. LHC bounds on third generation of scalar Leptoquarks. First and second plots show the constraints from ATLAS on $\sigma_{pp\to\phi\bar{\phi}} \times \mathcal{B}^2$ for third generation scalar Leptoquarks decaying to $t\tau$ or $b\tau$ [62]. Third one illustrates the bound from CMS on the cross-section for pair production of scalar Leptoquark with charge 1/3 at LHC considering $b\nu$ and $t\tau$ modes only [111]. The black dotted lines indicate the expected limits whereas the black solid lines with small squares (or the solid red lines) depict the observed limits. The green and yellow bands describe the 1σ and 2σ regions respectively over the expected limits. The black and blue dashed curve (along with brown and magenta shades on them) signify the theoretical prediction for the pair production of Leptoquarks (with theoretical uncertainties) with branching 100% and 23% respectively to a particular mode. (For interpretation of the colours in the figure(s), the reader is referred to the web version of this article.)

quarks. On the other hand, Fig. 1c depicts different bounds from CMS on vector Leptoquarks through the decay modes involving neutrinos.

The theoretically predicted curves, shown by brown bands in Figs. 1a, 1b and 1c, consider a Leptoquark to couple to a single generation of quark and lepton only indicating 100% branching fraction to a particular mode. But if the Leptoquarks are assumed to interact with all generations of quarks and leptons, the branching ratio in each generation diminishes. Consequently, the brown banded curves will now get scaled down as square of branching fraction, and they will intersect the experimental bands at lower masses than the earlier scenarios. For example, the magenta shaded curves signify the branching fraction to a particular mode to be 23% which obviously hit the experimental curves at lower masses than the brown strips. Additionally, the third and fourth plots of Fig. 1a confirms that adjustment in the branching fractions could allow us to work with Leptoquarks of a bit lower mass. Similarly, the plots in Fig. 1b signify that scalar Leptoquarks with masses above 1000 GeV are allowed with any branching fraction to third generation of quarks and leptons. We combine the CMS and ATLAS results from charged lepton modes in Fig. 2 to show the lower bounds (in TeV) on the mass of scalar leptoquark considering

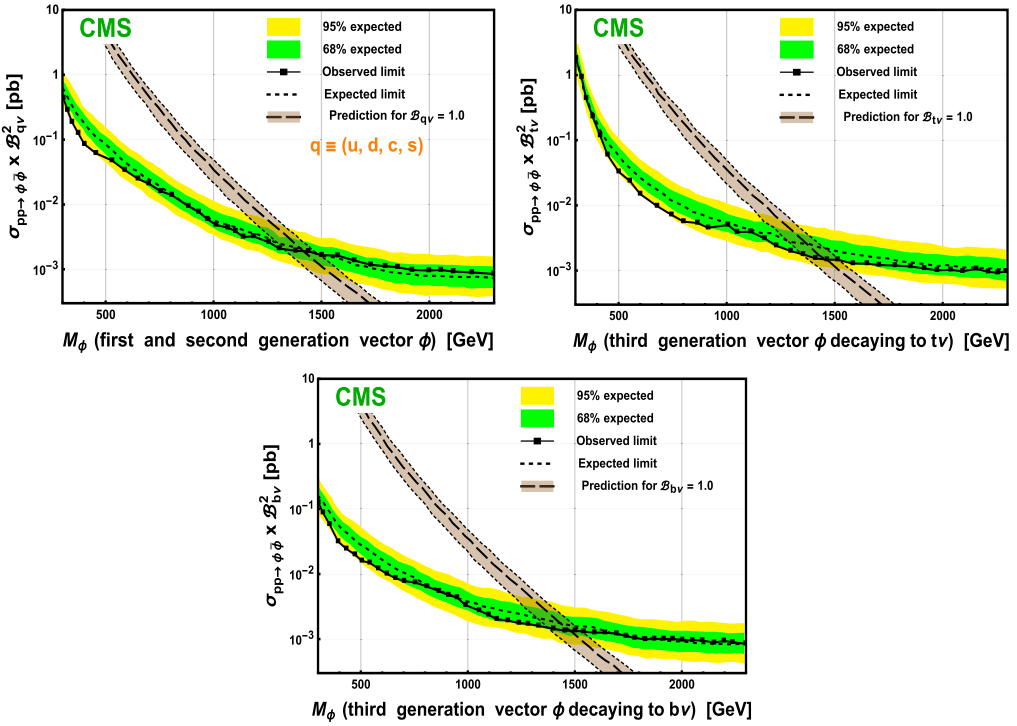

Fig. 1c. LHC bounds on vector Leptoquarks [68] from CMS considering the neutrino decay modes. While the first plot shows constraints on first two generations of vector Leptoquarks, the second and third plots depict the same for third generation. The black dotted lines indicate the expected limits whereas the black solid lines with small squares illustrate the observed limits for pair production of Leptoquarks at LHC. The green and yellow bands describe the 1σ and 2σ regions respectively over the expected limits. The black dashed curve (along with brown shade) depict the theoretical prediction for the pair production of Leptoquarks (with theoretical uncertainties) with branching 100% to a particular mode. (For interpretation of the colours in the figure(s), the reader is referred to the web version of this article.)

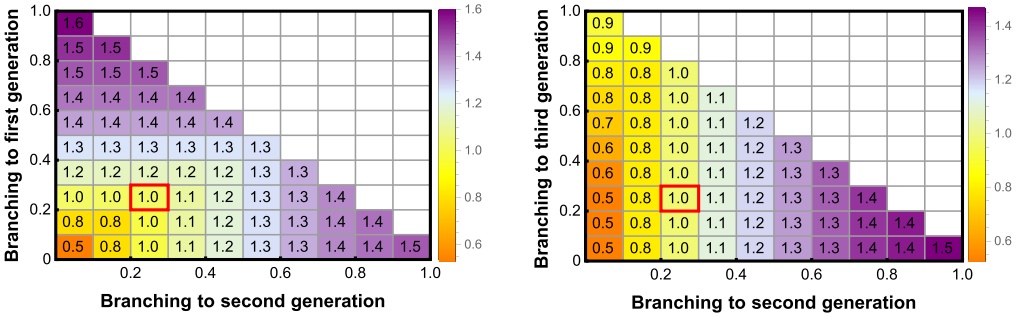

Fig. 2. Combined lower mass bound (in TeV) from ATLAS and CMS on scalar leptoquark decaying to all three generations of quarks and leptons using the charged lepton modes.

its decay to all three generations of quarks and leptons. On the other hand, bounds on vector Leptoquarks, shown in 1c, are on the invisible decay modes only.

Table 2
Benchmark points for Leptoquarks S_1 and $\widetilde{U}_{1\mu}$.

ϕ	BP	M_ϕ (GeV)	Y_L^{11}	Y_L^{22}	Y_L^{33}	Y_R^{11}	Y_R^{22}	Y_R^{33}
S_1	BP1	1000	0.2	0.2	0.2	0.2	0.2	0.2
	BP2	1500						
	BP3	2000						
$\widetilde{U}_{1\mu}$	BP1	1000	—	—	—	0.2	0.2	0.2
	BP2	1500						
	BP3	2000						

Table 3
Branching fractions of Leptoquarks S_1 and $\widetilde{U}_{1\mu}$ for the benchmark points specified in Table 2.

Modes	BP1	BP2	BP3	Modes	BP1	BP2	BP3
Leptoquark S_1				**Leptoquark $\widetilde{U}_{1\mu}$**			
$u\,e$	0.225	0.223	0.223	$e^+\,u$	0.338	0.336	0.335
$c\,\mu$	0.225	0.223	0.223	$\mu^+\,c$	0.338	0.336	0.335
$t\,\tau$	0.212	0.218	0.221	$t^+\,\tau$	0.323	0.329	0.331
$d\,\nu_e$	0.113	0.112	0.111	—	—	—	—
$s\,\nu_\mu$	0.113	0.112	0.111	—	—	—	—
$b\,\nu_\tau$	0.113	0.112	0.111	—	—	—	—

For our analysis, we have taken scalar singlet Leptoquark S_1 and vector singlet Leptoquark $\widetilde{U}_{1\mu}$ with masses 1 TeV, 1.5 TeV and 2 TeV respectively. The couplings (Y_L and Y_R) of these Leptoquarks with different generations of quarks and leptons are taken to be diagonal 3×3 matrices with entries 0.2, as shown in Table 2. It should be noted that both the couplings Y_L and Y_R exist for Leptoquark S_1, but there exists Y_R only for Leptoquark $\widetilde{U}_{1\mu}$ which can easily be seen from Table 1. It should also be noticed that our couplings are less than the electromagnetic coupling constant. The branching fractions of these Leptoquarks to different decay modes are listed in Table 3. The Leptoquark S_1 has around 23% branching to each of the charged lepton decay mode. It is assured from Fig. 1a that scalar Leptoquarks having 23% of branching fraction to first and second generations of quarks and leptons are allowed for all the three masses as considered in case of three BPs. Moreover, Fig. 1b indicates that these BPs are permitted while considering the bounds on scalar Leptoquarks that couple to third generation of quarks and leptons. One can also observe from Fig. 2 that scalar leptoquarks with branching 20% to 30% in each of the charged lepton modes, as depicted by the red box, should not be lighter than 1 TeV. On the other hand, the vector Leptoquark $\widetilde{U}_{1\mu}$ does not have any invisible decay mode, as shown in Fig. 1c, and hence there is no such direct bound on its mass.

4. Cross-section and angular distribution

In this section, we briefly discuss the theoretical aspects to determine the angular distribution as well as the total cross-section for the pair production of scalar and vector Leptoquarks in proton-proton collision [54]. Though these modes are accessible through photon and Z-boson mediated electroweak channels as well as the lepton mediated t-channel Feynman diagrams, for the sake of simplicity regarding theoretical calculations we neglect them. This presumption is justified since at very high energy the pair production of Leptoquark will be mostly QCD

dominated.[1] The Lagrangian related to the mass and kinetic part (QCD) of the scalar and vector Leptoquarks can be expressed as:

$$\mathcal{L}_s = \left(D^{\mu}_{ij}\,\phi^{j}_{s}\right)^{\dagger}\left(D^{ij}_{\mu}\,\phi_{s,j}\right) - M^2_{\phi_s}\,\phi^{i\,\dagger}_{s}\,\phi_{s,i}\ , \tag{4.1}$$

$$\begin{aligned}\mathcal{L}_v = &-\frac{1}{2}\,G^{i\,\dagger}_{\mu\nu}\,G^{\mu\nu}_{i} + M^2_{\phi_v}\,\phi^{i\,\dagger}_{v,\mu}\,\phi^{\mu}_{v,i} \\ &- i g_s\left[(1-\kappa_G)\,\phi^{i\,\dagger}_{v,\mu}\,T^{a}_{ij}\,\phi^{j}_{v,\nu}\,\mathcal{G}^{\mu\nu}_{a} + \frac{\lambda_G}{M^2_{\phi_v}}\,G^{i\,\dagger}_{\sigma\mu}\,T^{a}_{ij}\,G^{j\mu}_{\nu}\,\mathcal{G}^{\nu\sigma}_{a}\right],\end{aligned} \tag{4.2}$$

where $\phi_{s,v}$ are scalar and vector Leptoquarks with masses $M_{\phi_{s,v}}$, κ_G and λ_G are anomalous couplings, g_s is the strong coupling constant and T^a are the generators of $SU(3)$ colour gauge group. The covariant derivative as well as the field strength tensors for gluon ($\mathcal{A}_\mu$) and vector Leptoquark are given by:

$$D^{ij}_{\mu} = \partial_\mu\,\delta^{ij} - i g_s\,T^{ij}_{a}\,\mathcal{A}^{a}_{\mu}\ , \tag{4.3}$$

$$\mathcal{G}^{a}_{\mu\nu} = \partial_\mu\,\mathcal{A}^{a}_{\nu} - \partial_\nu\,\mathcal{A}^{a}_{\mu} + g_s\,f^{abc}\,\mathcal{A}_{\mu b}\,\mathcal{A}_{\nu c}\ , \tag{4.4}$$

$$G^{i}_{\mu\nu} = D^{ik}_{\mu}\,\phi_{v,\nu k} - D^{ik}_{\nu}\,\phi_{v,\mu k}\ . \tag{4.5}$$

Assuming all the quarks to be massless, the differential and integral partonic cross-sections for the pair production of scalar Leptoquark from gg and $q\bar{q}$ fusion becomes:

$$\begin{aligned}\frac{d\,\hat{\sigma}^{gg}_{s}}{d\cos\theta} = \frac{\pi\,\alpha_s^2\,\hat{\beta}}{6\,\hat{s}}\Bigg[&\frac{1}{32}\left(25 - 18\hat{\beta}^2 + 9\hat{\beta}^2\cos^2\theta\right) \\ &- \frac{1}{16}\left(\frac{25 - 34\hat{\beta}^2 + 9\hat{\beta}^4}{1-\hat{\beta}^2\cos^2\theta}\right) + \left(\frac{1-\hat{\beta}^2}{1-\hat{\beta}^2\cos^2\theta}\right)^2\Bigg],\end{aligned} \tag{4.6}$$

$$\hat{\sigma}^{gg}_{s} = \frac{\pi\,\alpha_s^2}{96\,\hat{s}}\left[\hat{\beta}\left(41 - 31\hat{\beta}^2\right) - \left(17 - 18\hat{\beta}^2 + \hat{\beta}^4\right)\log\left|\frac{1+\hat{\beta}}{1-\hat{\beta}}\right|\right], \tag{4.7}$$

$$\frac{d\,\hat{\sigma}^{q\bar{q}}_{s}}{d\cos\theta} = \frac{\pi\,\alpha_s^2}{18\,\hat{s}}\,\hat{\beta}^3\sin^2\theta \quad \text{and} \quad \hat{\sigma}^{q\bar{q}}_{s} = \frac{2\pi\,\alpha_s^2}{27\,\hat{s}}\,\hat{\beta}^3, \tag{4.8}$$

where $\hat{\beta} = \sqrt{1 - 4\,M^2_{\phi_s}/\hat{s}}$ and $\alpha_s = g_s^2/4\pi$ with $\hat{s}$ being the centre of mass energy and θ being the Leptoquark scattering angle in partonic CM frame.

However, the expression for pair production of vector Leptoquarks is not very simple and the angular distribution depends on the anomalous couplings κ_G and λ_G too. In this case, the angular distribution can be expanded in terms of polynomials of κ_G and λ_G, and the coefficients for the polynomial expansion can be expressed as functions of $s/M^2_{\phi_v}$, $\hat{\beta}$ and θ. Thus, the differential and integral partonic cross-sections for the pair production of vector Leptoquark from gg and $q\bar{q}$ fusion can be written as:

$$\frac{d\,\hat{\sigma}^{gg}_{v}}{d\cos\theta} = \frac{\pi\,\alpha_s^2\,\hat{\beta}}{192\,\hat{s}}\sum_{i=0}^{14}\chi^{g}_{i}(\kappa_G,\lambda_G)\,\frac{F_i(\hat{s},\hat{\beta},\cos\theta)}{(1-\hat{\beta}^2\cos^2\theta)^2}\ , \tag{4.9}$$

[1] For our simulation, we ignored the s-channel mediated electroweak processes, however, we do include the lepton mediated t-channel diagrams.

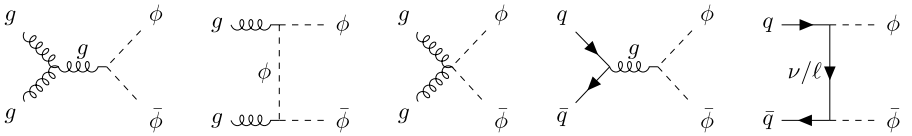

Fig. 3. Feynman diagrams for Leptoquark pair production at LHC. The photon and Z mediated diagrams have been ignored due to very small contribution.

$$\hat{\sigma}_v^{gg} = \frac{\pi\,\alpha_s^2}{96\,M_{\phi_v}^2} \sum_{i=0}^{14} \chi_i^g(\kappa_G, \lambda_G)\, \widetilde{F}_i(\hat{s}, \hat{\beta})\ , \tag{4.10}$$

$$\frac{d\,\hat{\sigma}_v^{q\bar{q}}}{d\cos\theta} = \frac{2\pi\,\alpha_s^2\,\hat{\beta}^3}{9\,M_{\phi_v}^2} \sum_{i=0}^{5} \chi_i^q(\kappa_G, \lambda_G)\, G_i(\hat{s}, \hat{\beta}, \cos\theta)\ , \tag{4.11}$$

$$\hat{\sigma}_v^{q\bar{q}} = \frac{4\pi\,\alpha_s^2\,\hat{\beta}^3}{9\,M_{\phi_v}^2} \sum_{i=0}^{5} \chi_i^q(\kappa_G, \lambda_G)\, \widetilde{G}_i(\hat{s}, \hat{\beta})\ , \tag{4.12}$$

$$\text{with} \quad \widetilde{F}_i = \frac{M_{\phi_v}^2}{\hat{s}} \int_0^{\hat{\beta}} d\xi\, \frac{F_i(\xi = \hat{\beta}\cos\theta)}{(1-\xi^2)^2} \quad \text{and} \quad \widetilde{G}_i = \int_0^1 d\cos\theta\, G_i(\hat{s}, \hat{\beta}, \cos\theta)\ . \tag{4.13}$$

However, it is important to mention that this expansion is model dependent and applicable to Leptoquarks with mass range of few hundred GeV to few TeV. Now, for minimal coupling scenario ($\kappa_G = 1,\ \lambda_G = 0$), we have:

$$\sum_{i=0}^{14} F_i\, \chi_i^g(\kappa_G = 1,\ \lambda_G = 0) = F_0 + F_1 + F_3 + F_6 + F_{10}\ , \tag{4.14}$$

$$\sum_{i=0}^{5} G_i\, \chi_i^g(\kappa_G = 1,\ \lambda_G = 0) = G_0 + G_1 + G_3\ . \tag{4.15}$$

The relevant F_i and G_i functions are listed in Appendix A. Finally, wrapping each partonic cross-section by corresponding parton distribution function (PDF) and summing over all such contributions, the total cross-section for pair production of Leptoquark at proton-proton collider is achieved. At this point, it is important to mention that the terms linear in κ_G and λ_G do not contain the unitarity violating factor s/M_ϕ^2 for gluon fusion channel; however, to restore the unitarity in quark fusion mode, the lepton exchanging t-channel diagrams must be included. On the other hand, if the energy is very high the Lagrangian for vector Leptoquark also needs to be corrected appropriately [54].

5. Distinguishing features of Leptoquarks

This section deals with distinguishing the features of different Leptoquarks from one another at LHC. In Fig. 3, we have shown the dominant Feynman diagrams for the pair production of Leptoquark at proton-proton collision. As expected, this process is mainly dominated by QCD. Hence, the tiny contributions from photon and Z mediated diagrams have been ignored.

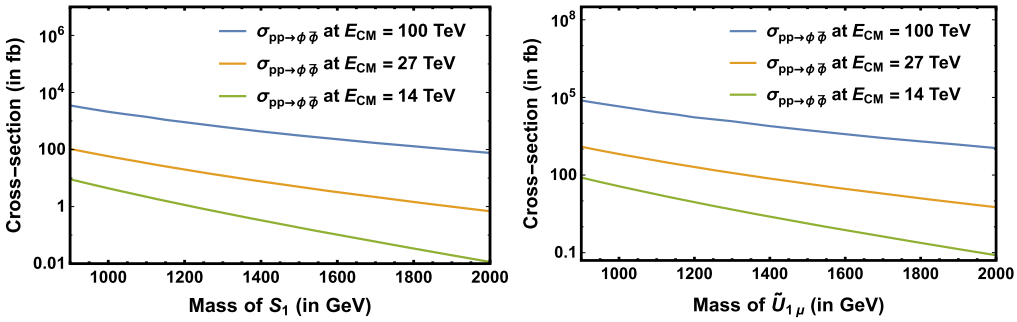

Fig. 4. Variation of hard scattering cross-sections for pair production of S_1 and $\widetilde{U}_{1\mu}$ with their masses in proton-proton collider for centre of momentum energies 14 TeV (green), 27 TeV (yellow) and 100 TeV (blue) respectively. (For interpretation of the colours in the figure(s), the reader is referred to the web version of this article.)

Table 4
Cross-section for pair-production of Leptoquarks S_1 and $\widetilde{U}_{1\mu}$ at LHC/FCC with different centre of momentum energies and benchmark points.

Benchmark points	Leptoquark S_1			Leptoquark $\widetilde{U}_{1\mu}$		
	Production cross-section in fb at different $\sqrt{s}$			Production cross-section in fb at different $\sqrt{s}$		
	14 TeV	27 TeV	100 TeV	14 TeV	27 TeV	100 TeV
BP1	4.38	58.03	2183.73	36.80	648.10	44636.30
BP2	0.18	4.91	320.40	1.34	45.79	5380.41
BP3	0.01	0.69	76.21	0.80	5.72	1116.03

5.1. Separating scalar and vector Leptoquarks

In this section, we focus on distinguishing the scalar Leptoquarks from their spin-1 vector counterparts. Since the pair-production of Leptoquark at LHC is QCD dominated, the production cross-section and the angular distribution remain practically independent of the gauge representation and electromagnetic charge of the Leptoquarks but depends on the spins. For convenience, we choose scalar singlet Leptoquarks S_1 and vector singlet Leptoquark $\widetilde{U}_{1\mu}$ with the masses and couplings specified in Table 2 and perform a PYTHIA based analysis. In order to study the angular distribution of the scattered Leptoquarks, we first reconstruct them from decay products (i.e. a charged and a quark) and then boost the whole system back in the rest frame of interaction.

5.1.1. Event rates of hard scattering cross-section:

In Fig. 4, we show the dependence of hard scattering cross-sections for pair production of S_1 (left panel) and $\widetilde{U}_{1\mu}$ (right panel) on their masses in proton-proton collision. The blue, yellow and green curves corresponds to the centre of momentum energy being 100 TeV, 27 TeV and 14 TeV respectively. As expected, the cross-section falls monotonically with increasing mass of Leptoquark and it increases with rise in energy of collision. It is important to notice that at any given $\sqrt{s}$ and M_ϕ, cross-section for production of vector Leptoquark is higher than that of scalar Leptoquark by order of magnitude. This happens because the vector Leptoquark has three different polarization states which enhance the cross-section for pair production by factor nine relative to the scalar one. It can also be observed from Table 4 which presents the hard scattering

cross-sections for pair production of scalar Leptoquark S_1 and vector Leptoquark $\widetilde{U}_{1\mu}$ for our chosen energies and benchmark points. For example, the hard scattering cross-sections for pair production of S_1 Leptoquark with mass 1 TeV and coupling 0.2 (BP1) at centre of momentum energies 14 TeV, 27 TeV and 100 TeV are 4.38 fb, 58.03 fb and 2183.73 fb respectively while the same for $\widetilde{U}_{1\mu}$ Leptoquark are 36.80 fb, 648.10 fb and 44636.30 fb respectively. Similarly, for BP3 the hard scattering cross-sections at the same centre of momentum energies with Leptoquark S_1 are 0.01 fb, 0.69 fb and 76.21 fb and the same with Leptoquark $\widetilde{U}_{1\mu}$ are 0.80 fb, 5.72 fb and 1116.03 fb respectively. So, just looking at the production cross-section, one can easily guess whether the produced Leptoquark is a scalar or vector one for the same final state topologies. It is worth mentioning that here we have demonstrated the results for vector Leptoquark in minimal coupling ($\kappa = 0$ or $\kappa_G = 1$) scenario. For Yang-Mills coupling the hard-scattering cross-section would be even higher [68].

5.1.2. Leptoquarks with same mass same decay at LHC

We analyse the $S_1^{1/3}$ and $\widetilde{U}_{1\mu}^{5/3}$ of identical mass, via their $c\mu$ decay modes at the LHC with centre of mass energies of 14, 27 and 100 TeV respectively by simulating the signal and dominant SM background via PYTHIA8 [102]. We summarize below the steps followed for the generation of events:

- A detailed simulation requires the models to be written in SARAH [103], which is then executed to generate the model files for CalcHEP [71,104].
- The ".lhe" events were then generated by CalcHEP using NNPDF2.3 [106] for parton distribution and fed into PYTHIA8 to account for the parton showering, hadronization and jet formation. The initial state and final state radiations (ISR/FSR) were switched on for the completeness of the analysis.
- We used Fastjet-3.2.3 [105] with jet radius of $\Delta R = 0.5$ using the anti-kT algorithm, constructed from the stable hadrons, and photons originated from the decay of neutral pions.
  - The calorimeter coverage is taken to be $|\eta| < 4.5, 2.5$ for the jets and leptons respectively.
  - A taggable lepton needs to be hadronically clean by demanding the hadronic activity within a cone of $\Delta R < 0.3$ around each lepton to be less than 15% of the leptonic transverse momentum (p_T).
  - The minimum p_T for the jets and leptons are demanded as 20 GeV with the respective criteria for the jet-lepton isolation ($\Delta R_{lj} > 0.4$) and the lepton-lepton isolation ($\Delta R_{ll} > 0.2$).
- The dominant SM backgrounds are also taken into account in order to estimate the signal significance at the LHC. We choose three benchmark points (BPs), with the Leptoquark masses 1.0 (BP1), 1.5 (BP2) and 2.0 (BP3) TeV respectively and Yukawa coupling 0.2 as mentioned in Table 2. To reduce the SM backgrounds we choose Leptoquark decays to $c\,\mu$ with respective branching fractions $\mathcal{B}(\phi_{s(v)} \to c\mu) = 0.23(0.33)$ for scalar (vector) Leptoquark for the rest of the analysis, as shown in Table 3, which are compatible with the LHC bounds [62–68].

For our purpose, we first boost back the lab frame to CM frame for which the reconstruction of the Leptoquark mass is necessary. We reconstruct the Leptoquark mass for each case from the invariant mass of jet, μ i.e. $M_{\ell j}$ as described in Figs. 5, 6 for the chosen benchmark points (in blue, green and purple) along with the dominant SM backgrounds (in orange) respectively. We consider all possible dominant SM backgrounds for the analysis, viz. $t\bar{t}$, $t\bar{t}V$, tVV, VV, VVV,

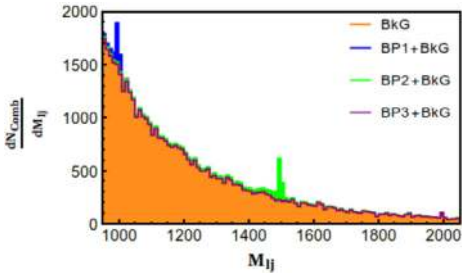

(a) S_1

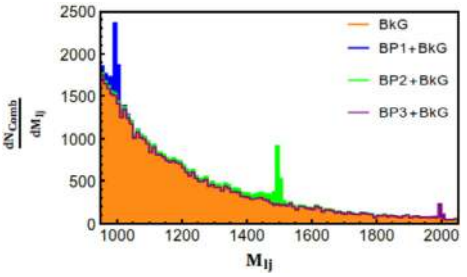

(b) $\widetilde{U}_{1\mu}$

Fig. 5. Invariant mass distributions of $j\mu$ for both scalar and vector Leptoquarks along with the dominant SM backgrounds at the LHC at 14 TeV.

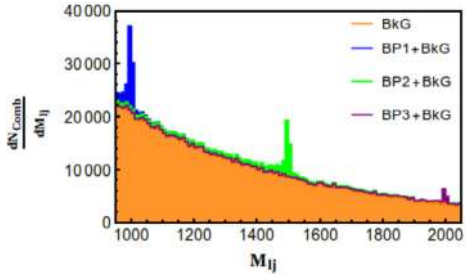

(a) S_1

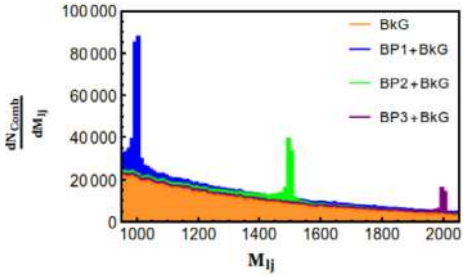

(b) $\widetilde{U}_{1\mu}$

Fig. 6. Invariant mass distributions of $j\mu$ for both scalar and vector Leptoquarks along with the dominant SM backgrounds at the LHC at 100 TeV.

where $V = Z,\ W^{\pm}$ and $tVV = tZW^-,\ \bar{t}ZW^+$. In order to obtain more statistics at higher values of jet-lepton invariant mass ($\gtrsim 1.0$ TeV), we imposed following cuts when generating background events: $M_{t\bar{t}} \geqslant 0.95,\ M_{t\bar{t}V} \geqslant 0.95,\ M_{tVV} \geqslant 0.95, M_{VV} \geqslant 0.95$ and $M_{VVV} \geqslant 0.95$ TeV. The tagging of high p_T muons along with a c-jet further reduces the Standard Model QCD backgrounds to a negligible level. Since SM backgrounds already depletes for high jet-lepton invariant mass at TeV scale, c-jet tagging and selection of high p_T muons have not been considered in our study. Due to large energy of interaction for the pp collision, the boost for the interacting partons are mostly longitudinal, thus for the reconstruction of CM frame, transverse boost has been neglected.

We summarize in the following, the criteria set for the selection of the final states:

- For our simulation, we select each event with $\geq 1\mu^+ + 1\mu^- + 2j$.
- In order to exclude backgrounds with an on-shell Z boson, we impose every combination of opposite charged leptons, and jets to satisfy $|M_{\ell\ell} - M_Z| > 5$, $|M_{jj} - M_Z| > 10$ GeV.
- We next take all possible combinations of the jet-lepton pairs and evaluate the invariant mass. The pairs originated from the Leptoquark decay will peak at the invariant mass of the Leptoquarks while the rest will form a continuum, whereas for the SM backgrounds the pattern show an exponential fall with the increase in the jet-lepton invariant mass as obtained in Figs. 5, 6.

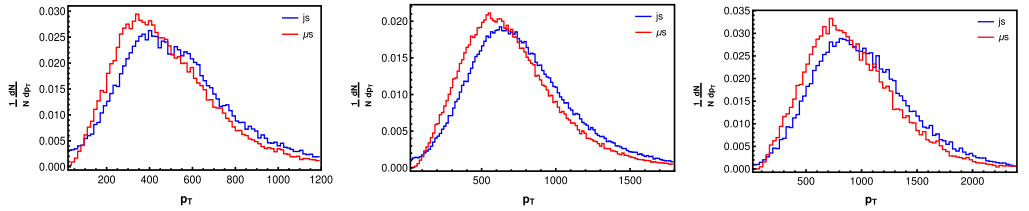

(a) BP1 (b) BP2 (c) BP3

Fig. 7. Transeverse momenta of the jets and leptons from the decay of the scalar Leptoquark S_1 pair produced at 14 TeV.

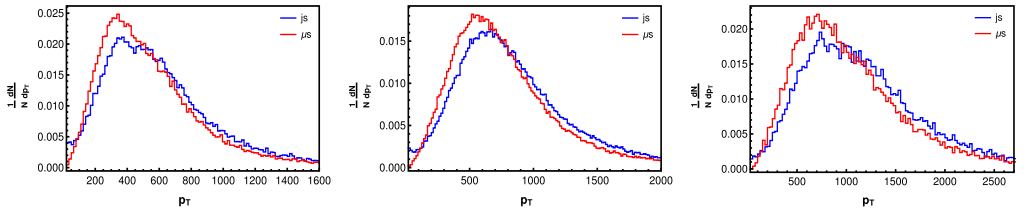

(a) BP1 (b) BP2 (c) BP3

Fig. 8. Transeverse momenta of the jets and leptons from the decay of the scalar Leptoquark S_1 pair produced at 100 TeV.

- Finally in order to obtain signals with a Leptoquark pair, we claim each event with exactly one pair of jet-lepton invariant mass satisfying $|M_{\mu^{\pm}j} - M_{\Phi}| \leq 10$ GeV. The sequential impositions of these cuts and their effects on Signal and Backgrounds has been enlisted in Tables 5, 6, 7.
- As discussed in Section 5.2.2, jet charge is an effective observable to discern different degenerate states of the same $SU(2)$ multiplet, and can optimise signatures of one member over the rest based on different Leptoquark decay modes leading to different event topologies. But in this section, since we focus on distinguishing two $SU(2)$ singlet Leptoquark with different spins having identical decay modes, we did not impose this cut.

In order to estimate the significance, the signal and the dominant SM background numbers are determined for all the Benchmark Points of the Signals in Tables 5, 6, 7 at an integrated luminosity of 1000 fb^{-1} at the LHC/FCC with centre of mass energies of 14, 27 and 100 TeV respectively. Obtaining the invariant Leptoquark mass from all possible combinations of invariant mass of the jet-lepton pairs for each event, and subsequent reconstruction of Leptoquark pair imposing the 10 GeV cut around the resonance peak is instrumental in reconstructing the centre of mass frame in which the angular distributions, as shown in Fig. 12 would exhibit patterns unique to the Leptoquark spins. With judicial imposition of cumulative cuts, we succeed to minimise the SM background to considerable proportion.

We begin our analysis with the kinematics of the Leptoquark decays. We select signal events with exactly 1 jet-muon and 1 jet-antimuon invariant masses falling within a 10 GeV window around the Leptoquark resonance peak as shown in Figs. 5, 6. We next plot the p_Ts of these jets (js), muons and antimuons (μs) as specified below. We observe that both the jet and muon p_Ts peak roughly around half the masses of the respective Leptoquarks, and this behaviour is independent of the Leptoquark spins. We present our results in Figs. 7, 8 for three benchmark

Table 5
Table displaying number of signal and background events after cumulative effect of cuts for different Benchmark Points at HL-LHC, for the centre of mass energy of 14 TeV at 1000 fb^{-1} of integrated luminosity.

BPs	Cuts	Signal		Background				
		S_1	$\widetilde{U}_{1\mu}$	$t\bar{t}$	$t\bar{t}V$	tVV	VV	VVV
BP1	$\geq 1\mu^+ + 1\mu^- + 2j$	163.91	2834.67	25526.21	243.19	26.48	543.26	116.47
	$+ \begin{cases} \lvert M_{\ell\ell} - M_Z \rvert > 5 \text{ GeV} \\ \lvert M_{jj} - M_Z \rvert > 10 \text{ GeV} \end{cases}$	119.87	2082.75	17089.94	154.27	10.46	83.19	26.91
	$+ \begin{cases} \lvert M_{\mu^- j} - M_\Phi \rvert \leq 10 \text{ GeV} \\ \lvert M_{\mu^+ j} - M_\Phi \rvert \leq 10 \text{ GeV} \end{cases}$	45.02	773.31	27.79	0.48	0.03	0.11	0.16
	Total	45.02	773.31			28.57		
	Sig	5.25	27.31			——		
	$\mathcal{L}_{5\sigma}$ (in fb^{-1})	907.03	33.52					
BP2	$\geq 1\mu^+ + 1\mu^- + 2j$	6.99	107.55	25526.21	243.19	26.48	543.26	116.47
	$+ \begin{cases} \lvert M_{\ell\ell} - M_Z \rvert > 5 \text{ GeV} \\ \lvert M_{jj} - M_Z \rvert > 10 \text{ GeV} \end{cases}$	5.23	83.21	17089.94	154.27	10.46	83.19	26.91
	$+ \begin{cases} \lvert M_{\mu^- j} - M_\Phi \rvert \leq 10 \text{ GeV} \\ \lvert M_{\mu^+ j} - M_\Phi \rvert \leq 10 \text{ GeV} \end{cases}$	1.82	27.56	1.60	0.02	0.002	0.00	0.02
	Total	1.82	27.56			1.64		
	Sig	0.98	5.10			——		
	$\mathcal{L}_{5\sigma}$ (in fb^{-1})	26030.82	961.17					
BP3	$\geq 1\mu^+ + 1\mu^- + 2j$	0.44	6.10	25526.21	243.19	26.48	543.26	116.47
	$+ \begin{cases} \lvert M_{\ell\ell} - M_Z \rvert > 5 \text{ GeV} \\ \lvert M_{jj} - M_Z \rvert > 10 \text{ GeV} \end{cases}$	0.34	4.79	17089.94	154.27	10.46	83.19	26.91
	$+ \begin{cases} \lvert M_{\mu^- j} - M_\Phi \rvert \leq 10 \text{ GeV} \\ \lvert M_{\mu^+ j} - M_\Phi \rvert \leq 10 \text{ GeV} \end{cases}$	0.11	1.48	0.15	0.004	0.0003	0.00	0.001
	Total	0.11	1.48			0.16		
	Sig	0.21	1.16			——		
	$\mathcal{L}_{5\sigma}$ (in fb^{-1})	566893.42	18579.07					

points at 14 and 100 TeV collision energies. We also observe the presence of longer tails for both jet and muon p_Ts for 100 TeV collisions, compared to the 14 TeV ones.

We also present, in Figs. 9 and 10, the jet and muon multiplicities of the signal events for all three different benchmark points and at 14 TeV and 100 TeV collisions. The multiplicities at different collision energies show similar patterns for different Leptoquark spins. We also observe that irrespective of the collision energies, di-muon final states are dominant. Also, due to the radiation effects, jet multiplicities peak roughly at 5 for both collision energies, irrespective of the Leptoquark mass. With our studies on kinematics performed, we next move on to the analysis of the signals and SM backgrounds for different benchmark points, at different collision energies.

Table 5 shows the number of signals and background events for a collision energy of 14 TeV, with an integrated luminosity ($\mathcal{L}_{int}$) of 1000 fb^{-1}. The cuts cumulatively imposed, optimise the signal events over the SM background. As discussed in Section 5.1.1, the vector Leptoquarks have larger cross-section for the pair-production, and thereby greater event rates over the scalar. The greater event rates for the vector Leptoquark $\widetilde{U}_{1\mu}$ over the scalar, S_1 are also reinforced by greater decay branching fraction to the second generation quark and muon ($\sim 33\%$) compared to the scalar one ($\sim 23\%$), as mentioned in Table 3. With the increase in the Leptoquark

Table 6
Table displaying number of signal and background events after cumulative effect of cuts for different Benchmark Points at FCC, for the centre of mass energy of 27 TeV at 1000 fb^{-1} of integrated luminosity.

BPs	Cuts	Signal		Background				
		S_1	$\widetilde{U}_{1\mu}$	$t\bar{t}$	$t\bar{t}V$	tVV	VV	VVV
BP1	$\geq 1\mu^+ + 1\mu^- + 2j$	2225.96	49592.87	136095.83	952.73	108.02	1282.24	1042.79
	$+ \begin{cases} \lvert M_{\ell\ell} - M_Z \rvert > 5 \text{ GeV} \\ \lvert M_{jj} - M_Z \rvert > 10 \text{ GeV} \end{cases}$	1555.52	34282.62	87006.97	499.01	52.26	205.64	521.29
	$+ \begin{cases} \lvert M_{\mu^- j} - M_\Phi \rvert \leq 10 \text{ GeV} \\ \lvert M_{\mu^+ j} - M_\Phi \rvert \leq 10 \text{ GeV} \end{cases}$	576.11	12882.17	56.56	1.40	0.85	4.03	1.77
	Total	576.11	12882.17			64.61		
	Sig	22.76	113.22			——		
	$\mathcal{L}_{5\sigma}$ (in fb^{-1})	48.26	1.95					
BP2	$\geq 1\mu^+ + 1\mu^- + 2j$	183.94	3432.36	136095.83	952.73	108.02	1282.24	1042.79
	$+ \begin{cases} \lvert M_{\ell\ell} - M_Z \rvert > 5 \text{ GeV} \\ \lvert M_{jj} - M_Z \rvert > 10 \text{ GeV} \end{cases}$	131.08	2451.09	87006.97	499.01	52.26	205.64	521.29
	$+ \begin{cases} \lvert M_{\mu^- j} - M_\Phi \rvert \leq 10 \text{ GeV} \\ \lvert M_{\mu^+ j} - M_\Phi \rvert \leq 10 \text{ GeV} \end{cases}$	45.62	882.63	4.01	0.05	0.04	0.99	0.46
	Total	45.62	882.63			5.56		
	Sig	6.38	29.62			——		
	$\mathcal{L}_{5\sigma}$ (in fb^{-1})	614.18	28.50					
BP3	$\geq 1\mu^+ + 1\mu^- + 2j$	25.73	414.49	136095.83	952.73	108.02	1282.24	1042.79
	$+ \begin{cases} \lvert M_{\ell\ell} - M_Z \rvert > 5 \text{ GeV} \\ \lvert M_{jj} - M_Z \rvert > 10 \text{ GeV} \end{cases}$	18.31	298.04	87006.97	499.01	52.26	205.64	521.29
	$+ \begin{cases} \lvert M_{\mu^- j} - M_\Phi \rvert \leq 10 \text{ GeV} \\ \lvert M_{\mu^+ j} - M_\Phi \rvert \leq 10 \text{ GeV} \end{cases}$	6.06	95.11	0.50	0.004	0.006	0.00	0.08
	Total	6.06	95.11			0.59		
	Sig	2.35	9.72			——		
	$\mathcal{L}_{5\sigma}$ (in fb^{-1})	4526.94	264.61					

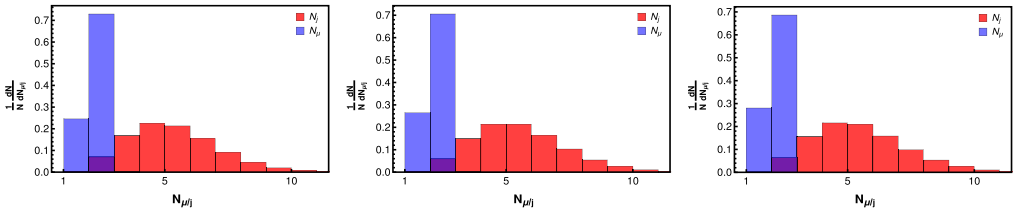

(a) BP1 (b) BP2 (c) BP3

Fig. 9. Multiplicity of the jets and muons for the pair production of the scalar Leptoquark S_1 at 14 TeV.

mass, the event rates for the signal fall down, along with an exponential decrease in total background events, apparent from the Figs. 5, 6 due to imposition of high jet-muon invariant mass requirement.

As the data suggests, the signal significances for the vector singlet Leptoquark pair production is roughly five times to that for the scalar singlet, in compliance with the factors discussed above.

Table 7
Table displaying number of signal and background events after cumulative effect of cuts for different Benchmark Points at FCC, for the centre of mass energy of 100 TeV at 1000 fb^{-1} of integrated luminosity.

BPs	Cuts	Signal		Background				
		S_1	$\widetilde{U}_{1\mu}$	$t\bar{t}$	$t\bar{t}V$	tVV	VV	VVV
BP1	$\geq 1\mu^+ + 1\mu^- + 2j$	55706.1	2500796.2	2500301.8	6463.6	1412.1	19969.4	2355.9
	$+ \begin{cases} \lvert M_{\ell\ell} - M_Z\rvert > 5 \text{ GeV} \\ \lvert M_{jj} - M_Z\rvert > 10 \text{ GeV} \end{cases}$	37971.4	1665106.2	1553908.9	3354.9	806.2	1190.3	630.8
	$+ \begin{cases} \lvert M_{\mu^- j} - M_\Phi\rvert \leq 10 \text{ GeV} \\ \lvert M_{\mu^+ j} - M_\Phi\rvert \leq 10 \text{ GeV} \end{cases}$	13976.6	663855.1	292.2	18.3	6.2	13.9	6.6
	Total	13976.6	663855.1			337.2		
	Sig	116.8	814.6			———		
	$\mathcal{L}_{5\sigma}$ (in fb^{-1})	1.83	0.04					
BP2	$\geq 1\mu^+ + 1\mu^- + 2j$	10138.3	348740.3	2500301.8	6463.6	1412.1	19969.4	2355.9
	$+ \begin{cases} \lvert M_{\ell\ell} - M_Z\rvert > 5 \text{ GeV} \\ \lvert M_{jj} - M_Z\rvert > 10 \text{ GeV} \end{cases}$	6923.8	237557.8	1553908.9	3354.9	806.2	1190.3	630.8
	$+ \begin{cases} \lvert M_{\mu^- j} - M_\Phi\rvert \leq 10 \text{ GeV} \\ \lvert M_{\mu^+ j} - M_\Phi\rvert \leq 10 \text{ GeV} \end{cases}$	2364.3	82965.4	45.2	2.2	1.5	9.3	1.9
	Total	2364.3	82965.4			60.1		
	Sig	48.0	287.9			———		
	$\mathcal{L}_{5\sigma}$ (in fb^{-1})	10.84	0.30					
BP3	$\geq 1\mu^+ + 1\mu^- + 2j$	2088.7	130571.7	2500301.8	6463.6	1412.1	19969.4	2355.9
	$+ \begin{cases} \lvert M_{\ell\ell} - M_Z\rvert > 5 \text{ GeV} \\ \lvert M_{jj} - M_Z\rvert > 10 \text{ GeV} \end{cases}$	1431.5	87408.9	1553908.9	3354.9	806.2	1190.3	630.8
	$+ \begin{cases} \lvert M_{\mu^- j} - M_\Phi\rvert \leq 10 \text{ GeV} \\ \lvert M_{\mu^+ j} - M_\Phi\rvert \leq 10 \text{ GeV} \end{cases}$	468.7	29548.9	8.2	0.5	0.3	2.8	0.3
	Total	468.7	29548.9			12.3		
	Sig	21.3	171.9			———		
	$\mathcal{L}_{5\sigma}$ (in fb^{-1})	55.10	0.85					

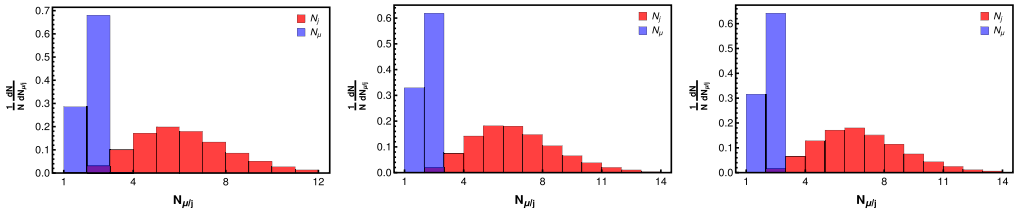

(a) BP1 (b) BP2 (c) BP3

Fig. 10. Multiplicity of the jets and muons for the pair production of the scalar Leptoquark S_1 at 100 TeV.

For the probe of both scalar and vector Leptoquarks for different benchmark points at 14 TeV LHC, a 5σ discovery can be achieved for 1 TeV vector Leptoquark $\widetilde{U}_{1\mu}$ at a relatively early stage of high luminosity LHC (HL-LHC) run, for an integrated luminosity of 34 fb^{-1}, while 1 TeV scalar, S_1 requires ~ 910 fb^{-1} to achieve 5σ significance.

For 1.5 TeV vector Leptoquark probe at 14 TeV, an integrated luminosity of 960 fb^{-1} is required for the 5σ significance while, an integrated luminosity of $\sim 26 \times 10^3$ fb^{-1} is required for the 5σ significance of S_1. 2.0 TeV $\widetilde{U}_{1\mu}$ requires $\sim 18 \times 10^3$ fb^{-1} whereas, S_1 with identical mass requires $\sim 566 \times 10^3$ fb^{-1} of dataset to achieve a 5σ significance. Certainly their discovery, or ruling out necessitates greater size of the dataset and can therefore might be possible at the later phase of HL-LHC run.

The next table, Table 6 shows the number of signals and background events at 27 TeV collision with an integrated luminosity ($\mathcal{L}_{int}$) of 1000 fb^{-1} for all three benchmark points. Comparing with Table 5, we observe that an increase in collision energy increases the event rates manyfold depending on the leptoquark mass and spins, although the ratio of signal significance of the vector singlet to that of the scalar singlet leptoquarks roughly retains the same value. We observe that, a 5σ discovery can be achieved for both scalar and vector leptoquarks of masses 1.0 and 1.5 TeV at fairly earlier stage of the run. An integrated luminosity of ~ 1.95 fb^{-1} is required for 5σ discovery of 1.0 TeV $\widetilde{U}_{1\mu}$, while the same for S_1 requires ~ 48.26 fb^{-1}. For the 1.5 TeV mass, $\widetilde{U}_{1\mu}$ requires ~ 28.5 fb^{-1} and S_1 requires ~ 614.2 fb^{-1} of integrated luminosities to be probed with 5σ significance. The 2.0 TeV $\widetilde{U}_{1\mu}$ would require a dat set of size ~ 264.61 fb^{-1} and S_1 would require that of ~ 4.5 ab^{-1} for 5σ discovery.

Finally, we present, in Table 7, the event rates for signals and background for a 100 TeV collision with an integrated luminosity ($\mathcal{L}_{int}$) of 1000 fb^{-1} for all three BPs. The ratio of the signal significances of the vector $\widetilde{U}_{1\mu}$ to the scalar S_1 for different benchmark points roughly amounts to 7. It is evident that an earlier stage of FCC run will be able to discover or rule out the Leptoquarks of all three BPs, of both spins. An integrated luminosity of $\sim$38 pb^{-1} would lead to a signal significance of 5σ for 1.0 TeV $\widetilde{U}_{1\mu}$, $\sim$0.3 fb^{-1} for 1.5 TeV $\widetilde{U}_{1\mu}$ and of $\sim$0.9 fb^{-1} for 2.0 TeV $\widetilde{U}_{1\mu}$. Similarly, an integrated luminosity of $\sim$1.8 fb^{-1} would lead to the same for 1.0 TeV S_1, $\sim$10.8 fb^{-1} for 1.5 TeV S_1 and of $\sim$55 fb^{-1} for 2.0 TeV S_1.

5.1.3. Angular distribution

Before going to the simulation of angular distribution at LHC, let us first discuss the theoretical description of the parton level contributions. We investigate the contributions from quarks and gluons in the normalized angular distribution of Leptoquark pair production at LHC for both scalar and vector Leptoquarks with respect to the angle (θ) between produced Leptoquark and the beam axis in the centre of momentum (CM) frame. The QCD contributions to the hard scattering cross-sections and angular distributions for these processes are already discussed in Section 4. However, in this section we incorporate the lepton mediated t-channel diagrams also.

The Feynman Diagrams for pair production of Leptoquark at LHC are presented in Fig. 3. In Figs. 11a and 11b, we summarize the parton level angular distributions normalized to the respective cross-sections for scalar and vector Leptoquarks in the CM frame. While Fig. 11a displays the contributions from quarks and gluons in the angular distributions for pair production of scalar Leptoquarks at three different values of $\sqrt{s}$ for M_ϕ =1.5 TeV and the quark-lepton-Leptoquark coupling being 0.2 for all the three generations of fermions, Fig. 11b exhibits the same for vector Leptoquarks with minimal coupling ($\kappa_G = 1,\ \lambda_G = 0$) [54]. Though bounds from LEP [55], HERA [56], CERN [57] and Tevatron [58,59] indicate that there is still little room for low mass Leptoquark with appropriate branching to different generations of fermions [60,61], we take a conservative approach, and considering the constraints from ATLAS [62,63] and CMS [64–68] only we choose the above mentioned benchmark point. In the first plots of Fig. 11a and 11b, we consider the pair production of Leptoquark from that quark (one generation) only whose left and right both chiral components couple to the Leptoquark, e.g. the contribution of u-quark

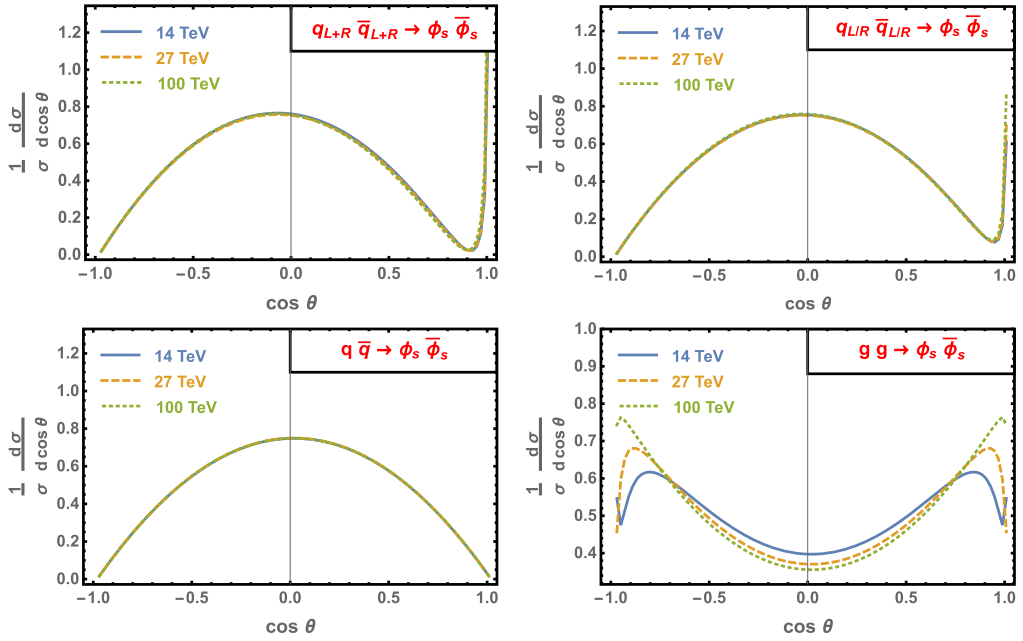

Fig. 11a. Parton level angular distribution normalized to their cross-sections for pair production of scalar (ϕ_s) Leptoquarks in the CM frame taking $M_\phi = 1.5$ TeV and quark-lepton-Leptoquark coupling to be 0.2. The blue (solid), orange (dashed) and green (dotted) line indicate the distribution at $\sqrt{s}$ being 14 TeV, 27 TeV and 100 TeV respectively. The first, second and third plots show contributions of quarks under three different scenarios, respectively: a) when both left and right handed quark couple to Leptoquark, b) when quark couples to Leptoquark through one chirality only, c) when Leptoquark does not couple to a particular quark at all. The fourth one exhibits the distribution for gluon fusion channel.

in the pair production of S_1 or that of d-quark in the pair production of $U_{1\mu}$, and we denote it as q_{L+R}. In the second plots of Fig. 11a and 11b, we show the effects of the quark (one generation) that couples to the Leptoquark through one chirality only, for example the pair production of $\widetilde{S}_1$ from $d\,\bar{d}$ as $\widetilde{S}_1$ couples to d_R^c only or that of $\widetilde{U}_{1\mu}$ from the fusion of u-quark, and we write it as $q_{L/R}$. Similarly, in the third plots of both the figures, we represent the contribution from the quark which does not couple to the Leptoquark at all and the pair production happens through gluon mediated s-channel diagram only, e.g. production of $\widetilde{S}_1$ from $u\bar{u}$ channel or production of $\widetilde{U}_{1\mu}$ from $d\bar{d}$ mode. One can easily notice the tiny effects of lepton-mediated t-channel diagrams around $\cos\theta \sim 1$ in first and second columns while comparing them with the third one. It is worth mentioning that we have not considered contributions from photon and Z^0 mediated s-channel processes since their distributions are quite similar to the gluon-mediated one but with very small magnitude. Finally in the fourth plots we exhibit the angular distributions for Leptoquark pair production from gluon fusion. It can be seen that the distribution for scalar Leptoquark production in gluon fusion increases at both sides of $\cos\theta = 0$. However, near $\cos\theta \sim \pm 1$, it attains maximum and starts decreasing, then it reaches minimum and starts increasing rapidly around the edge of phase space. Though it is difficult to observe the minimum for higher values of $\sqrt{s}$, since it is too close to $\cos\theta = \pm 1$, the maximum is clearly visible. This effect disappears for $\hat{\beta} < 0.908$ and we get a monotonically increasing curve on both sides of $\cos\theta = 0$.

The above effects, however, is bound to change at the real colliders due the effects of parton distribution function as well as the energies. The asymmetric behaviour of angular distribution

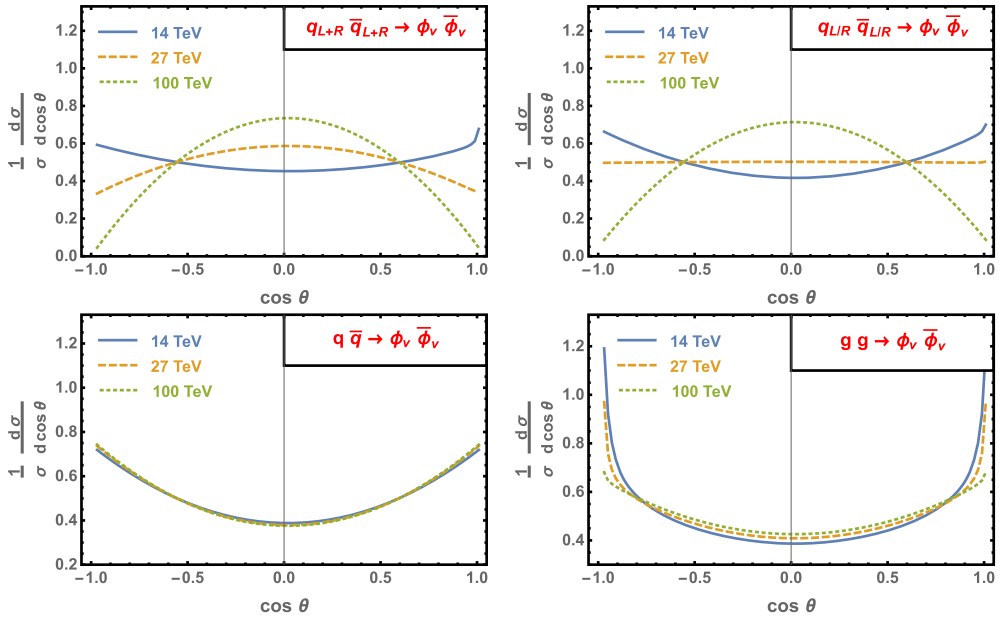

Fig. 11b. Parton level angular distribution normalized to their cross-sections for pair production of vector (ϕ_v) Leptoquarks in the CM frame taking $M_\phi = 1.5$ TeV and quark-lepton-Leptoquark coupling to be 0.2. The blue (solid), orange (dashed) and green (dotted) line indicate the distribution at $\sqrt{s}$ being 14 TeV, 27 TeV and 100 TeV respectively. The first, second and third plots show contributions of quarks under three different scenarios, respectively: a) when both left and right handed quark couple to Leptoquark, b) when quark couples to Leptoquark through one chirality only, c) when Leptoquark does not couple to a particular quark at all. The fourth one exhibits the distribution for gluon fusion channel.

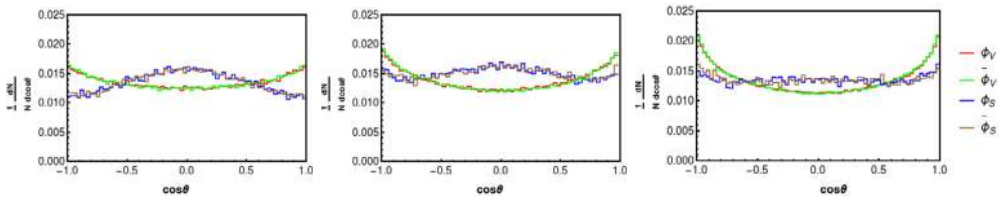

(a) 14 TeV (b) 27 TeV (c) 100 TeV

Fig. 12. Normalised angular distribution of the 1.5 TeV scalar and vector Leptoquark pairs (BP2) for three different collision energies after correction for longitudinal boost effect. The plots are made with the events lying within 10 GeV window of Leptoquark invariant mass peak, *i.e.,* after imposing the final cut on signals and backgrounds in Table 5, 6 and 7.

in quark fusion channels will also be symmetrized in actual proton-proton collision since inside each proton there are quarks and anti-quarks distributed according to parton distribution function. For our choices of $\sqrt{s}$ and Leptoquark mass in pp collision at the LHC the tail effects near $\cos\theta \sim \pm 1$ are diminished. Now, we shall analyse the total cumulative effects of quarks and gluon fusion leading to Leptoquark pair production and the angular distribution of the Leptoquarks in CM frame.

Equipped with the CM frame we reconstruct the angular distribution with respect to angle θ, the angle between the incoming parton and Leptoquark (anti-Leptoquark). The Leptoquark

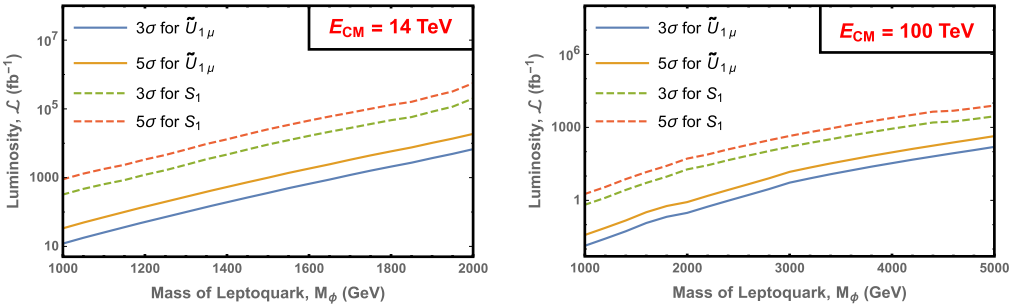

Fig. 13. Required integrated luminosity for finding Leptoquarks $\widetilde{U}_{1\mu}$ and S_1 with 3σ and 5σ significances as function of their mass at centre of momentum energy being 14 TeV (panel) and 100 TeV (right panel). The couplings are taken as described in Table 2 for all masses of the Leptoquarks. The 3σ and 5σ contours for vector singlet Leptoquark $\widetilde{U}_{1\mu}$ are indicated by blue and yellow solid lines whereas the same for scalar singlet Leptoquark S_1 are shown by green and red dashed curves respectively. (For interpretation of the colours in the figure(s), the reader is referred to the web version of this article.)

(anti-Leptoquark) can be identified via the presence of $\mu^-(\mu^+)$ in the final states while reconstructing the Leptoquarks masses. The angular distributions for the scalar S_1 and vector $\widetilde{U}^{5/3}_{1\mu}$ Leptoquarks are shown in Fig. 12. The red (green) coloured are for the vector-like Leptoquark (anti-Leptoquark); whereas the blue (brown) are for the scalar Leptoquark (anti-Leptoquark) respectively. We note that the subprocess displayed in first two plots of Fig. 11a and 11b contribute to the pair production with a strength of fourth power of Yukawa coupling coefficient while, the subprocesses in the last two column is QCD mediated and contribute with a strength of fourth power of strong coupling coefficient. Hence, the effect in angular distribution pattern induced by Yukawa-mediated cross-channels are suppressed in comparison to QCD-mediated s-channel processes. The final angular distribution of the scatter Leptoquark pair is thus dominated by cumulative contribution of s-channel fusions. The gluon fusion contributes to a trough for scattering angles (θ) close to $\pi/2$ and a trough for $\theta \sim 0, \pi$. For quark pair fusion the effect is reverse. We could see that for scalar Leptoquark, though the final angular distribution in pp collision mimics the shape of quark pair annihilation process in the central region (low $|cos\theta|$), it gets more contribution from gluon fusion in the peripheral portion (high $|cos\theta|$) of phase space (see Fig. 11a and 11b). For reasons discussed above, the tail-effects in angular distribution of scalar pair are also diminished due to parton distribution function. However, for vector Leptoquark the angular distribution is mostly dominated by gluon fusion. Nevertheless, it is clear from Fig. 12 that the scalar and vector Leptoquarks can be segregated via their angular distribution in the reconstructed CM frame. Fig. 12 (a), (b), (c) describe the angular distributions at the LHC and FCC with centre of mass energies of 14, 27 and 100 TeV respectively. For the chosen Leptoquark mass of 1.5 TeV, we see such discerning of spins of Leptoquarks are possible even when they generate the similar final state.

5.1.4. Leptoquark reaches at LHC/FCC

As evident from Tables 5, 6 and 7, for similar masses, couplings and collision energies, the vector Leptoquarks have larger significance than their scalar counterparts. As discussed earlier, three polarizations contributing to three degrees of freedom for vector Leptoquarks increase its pair-production cross-section, thereby increasing the signal significance. Hence, comparatively a lower luminosity will be required to achieve 5σ significance for the vector Leptoquarks. There-

Table 8
Required integrated luminosity to observe pair-production of Leptoquarks S_1 and $\widetilde{U}_{1\mu}$ at LHC/FCC with 5σ significance for different centre of momentum energies and benchmark points.

Benchmark points	Leptoquark S_1			Leptoquark $\widetilde{U}_{1\mu}$		
	Required luminosity in fb^{-1} for 5σ significance at different $\sqrt{s}$			Required luminosity in fb^{-1} for 5σ significance at different $\sqrt{s}$		
	14 TeV	27 TeV	100 TeV	14 TeV	27 TeV	100 TeV
BP1	0.91×10^3	48.26	1.83	33.52	1.95	0.04
BP2	2.60×10^4	0.61×10^3	10.84	0.96×10^3	28.50	0.30
BP3	5.67×10^5	4.53×10^3	55.10	1.86×10^4	0.26×10^3	0.85

fore, they will be discovered or ruled out at much earlier stage of the run compared to the scalar ones.

In Fig. 13, we present plots showing integrated luminosities (in fb^{-1}) required for achieving signal significances of 3σ and 5σ respectively at 14 TeV (at the left) and 100 TeV (at the right) collisions as a function of the Leptoquark mass. We have considered the spin-0 S_1 and spin-1 $\widetilde{U}_{1\mu}$ with their decays to the second generation quark and lepton with the branching fraction mentioned in Table 3. The blue and yellow solid lines indicate 3σ and 5σ contours for $\widetilde{U}_{1\mu}$ whereas the green and red dashed lines describe the same for S_1. As expected, the scalar Leptoquark S_1 needs much higher luminosity to be probed with an appreciable significance than the vector Leptoquark $\widetilde{U}_{1\mu}$. Required integrated luminosity to observe pair-production of Leptoquarks S_1 and $\widetilde{U}_{1\mu}$ at LHC/FCC with 5σ significance for different centre of momentum energies and benchmark points are also tabulated in Table 8. As can be seen, in order to achieve 5σ significance for Leptoquark S_1 with BP1 at centre of momentum energies 14 TeV and 100 TeV one needs integrated luminosities of 907 fb^{-1} and 1.83 fb^{-1} respectively whereas for the same with Leptoquark $\widetilde{U}_{1\mu}$, one requires integrated luminosities of 33.5 fb^{-1} and 0.04 fb^{-1} respectively. Similarly, to reach 5σ significance at the same centre of momentum energies for BP3 with Leptoquark S_1, luminosities of 5.67×10^5 fb^{-1} and 55.10 fb^{-1} are needed while for the same with Leptoquark $\widetilde{U}_{1\mu}$, luminosities of 1.86×10^4 fb^{-1} and 0.85 fb^{-1} are required respectively. It should also be noticed from Fig. 13 that with 1000 fb^{-1} of integrated luminosity and 14 TeV of centre of momentum energy, one can probe vector Leptoquark $\widetilde{U}_{1\mu}$ (with minimal coupling) up to mass 1.5 TeV with 5σ significance while one cannot go much beyond 1 TeV of mass for scalar Leptoquark S_1. On the other hand, at 100 TeV of centre of momentum energy with 1000 fb^{-1} of integrated luminosity, vector Leptoquark $\widetilde{U}_{1\mu}$ of 5 TeV mass can easily be probed at LHC with same significance whereas scalar Leptoquark S_1 can be probed till mass 3.5 TeV only.

5.2. *Differentiating Leptoquarks with same spin*

Having discussed the segregation of different Leptoquarks based on spins, which affect uniquely, the distribution of the scattered states at rest frame of interaction, we now concentrate on distinguishing different Leptoquark with the same spin, but with different electromagnetic charges and $SU(2)$ representations.

5.2.1. *Different $SU(2)_L$ or $U(1)$ representation*

Apart from the singlet Leptoquarks, there are also other Leptoquarks in the doublet and triplet representations of $SU(2)_L$ for the cases of scalar (R_2, $\widetilde{R}_2$, $\vec{S}_3$) and vectors ($V_{2\mu}$, $\widetilde{V}_{2\mu}$, $\vec{U}_{3\mu}$) as shown in the Table 1. All of these Leptoquarks have $SU(2)_L$ partners with same tree-level

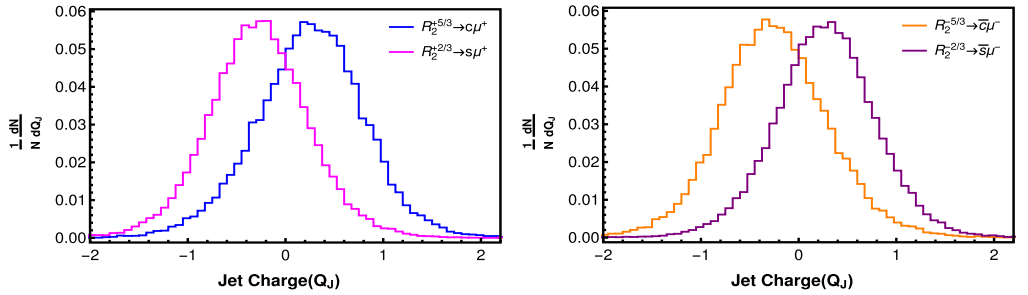

(a) Produced with μ^+ (b) Produced with μ^-

Fig. 14. Charge of the jets from the decay of the scalar doublet Leptoquarks R_2 pair produced at 14 TeV.

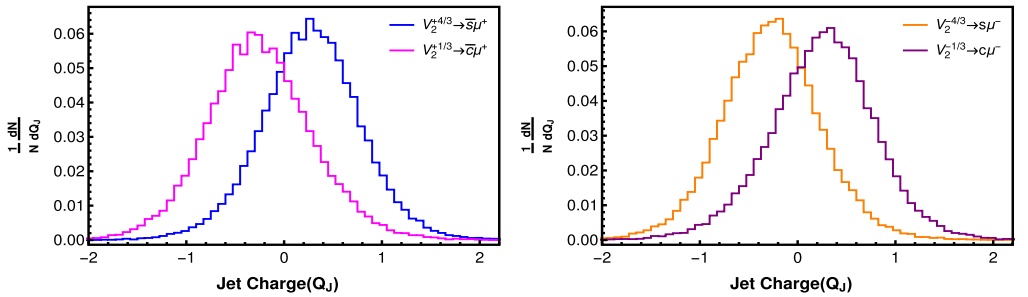

(a) Produced with μ^+ (b) Produced with μ^-

Fig. 15. Charge of the jets from the decay of the vector doublet Leptoquarks $V_{2\mu}$ pair produced at 14 TeV.

mass but have different final state topologies. As an illustration, let us consider the example of $\vec{S}_3$ ($\vec{U}_{3\mu}$), with components $S_3^{+4/3}$, $S_3^{+1/3}$ and $S_3^{-2/3}$ ($U_{3\mu}^{+5/3}$, $U_{3\mu}^{+2/3}$ and $U_{3\mu}^{-1/3}$). The last component of $SU(2)_L$ multiplet decays only to anti-up (down) type quarks and anti-neutrinos and thus has topology distinct from the first two members. The first component decays only to the charged anti-lepton and anti-down (up) type quark while the second one decays to charged anti-lepton anti-up (down) type quarks and antineutrino anti-down (up) type quarks simultaneously. The first two members of the weak isospin multiplet shows complementary signatures while the third one shows semi-invisible mode. Determination of electromagnetic charge of jet originated from Leptoquark decay has been shown instrumental in segregating such complimentary jet final states [60]. Observations of such complementary modes with decay to charged leptons and quarks can eventually distinguish different gauge representation within the same spin group (scalar or vector). Precisely, Leptoquarks (or, anti-Leptoquarks) with electromagnetic charge, $-1 < Q_\phi < 0$ have zeros in their angular distribution in electron-photon collider [61] while others, with $|Q_\phi| > 1$ can manifest similar phenomena at electron-hadron collider when produced in association with a photon in the final state [60].

5.2.2. *Jet charge*

In case of doublet and triplet Leptoquarks, different components of same multiplet will be produced simultaneously at LHC due to degeneracy of their respective masses. Then it becomes important to distinguish the signatures of different excitations of same multiplet. Determina-

tion of the charge for the jets [107–109] produced from the decay of the Leptoquarks turns out to be instrumental in this regard. For example, the scalar doublet Leptoquark R_2 consists of two components, $R_2^{+5/3}$ and $R_2^{+2/3}$ which would eventually decay to $c\mu^+$ and $s\mu^+$ respectively (considering decay to second generation of fermions only). Hence, if one tags the μ^+ and determines the charge of the jet produced with it,[2] it will be seen that the charge of jet from $R_2^{+5/3}$ peaks around $+0.4$ whereas the same from $R_2^{+2/3}$ peaks at -0.3 which can be observed from the left panel of Fig. 14. Similarly, in case of $\bar{R}_2$ (anti-particle of R_2), the jet produced along with μ^- should be considered for charge determination. However, the results will be opposite to previous case, as shown in the right panel of Fig. 14, since $R_2^{-5/3}$ produces $\bar{c}$ while $R_2^{-2/3}$ creates $\bar{s}$. Same study for the vector doublet Leptoquark $V_{2\mu}$, produced at proton-proton collision at 14 TeV has been depicted in Fig. 15. Thus different members of same weak isospin multiplet can be isolated using the technique of jet charge determination.

6. Conclusion

In this paper, we have studied how to distinguish the signatures of different Leptoquarks, if they are produced in proton-proton collision at LHC/FCC. This involves the discrimination of the spin as well as the gauge representations. The information of the spin representations is encoded in their production cross-sections. For example the production cross-sections are a few times higher for vector Leptoquarks compared to the scalar ones for the choices of the same mass at the LHC/FCC, specially for the hadronic collider where the productions are mostly by the strong interactions. Higher degree of freedom of vector Leptoquarks thus will have early signals at the LHC and FCC.

The spin information can also be probed directly by reconstructing the centre of mass frame as shown in this article. The muon and the jet coming from the Leptoquark decay can be identified via their invariant mass peak which also enables us to reconstruct the CM frame. It is shown that the angular distributions of the cosine of the angle of Leptoquarks with the beam axis for scalar takes a convex shape while for the vector ones it follows a concave one. The departure from the matrix element calculation to the proton proton collision with the effects of parton distribution functions are also discussed.

The situation gets even more interesting for higher gauge representations like $SU(2)$ doublets or triplets as they come with more partners within the same mass. However, as pointed out that different dominant decay modes will lead to different final state topologies which ease out the differentiation. In this context we also showed how the reconstruction of the jet charge from the hadronic constituents can pinpoint the decays of the Leptoquarks involved.

Finally we also estimate the required luminosity to probe the scalar and vector Leptoquarks in the TeV range. It is noticed that the LHC with 100 TeV centre of mass energy and with an integrated luminosity of 1000 fb^{-1} can probe the scalar Leptoquark of mass ~ 3.5 TeV. For the same LHC specifications mass of $\gtrsim 5$ TeV can be probed for the vector Leptoquarks. We showed how different such disntiguishers can be instrumental in discerning Leptoquarks with different spin and same gauge representations and vice-versa at the LHC/FCC.

[2] The invariant mass of jet-μ^+ pair would peak around the Leptoquark mass if they come from same Leptoquark.

CRediT authorship contribution statement

The paper is carried out by the mutual efforts of all the authors involved in it. From the idea conceptualization, methodology and some of the simulation checks along with the supervision of the project was done by Priyotosh Bandyopadhyay. Mahesh Jakkapu was involved in the initial state of the projects and did some crucial checks. PYTHIA8 plus FastJet simulations are done by Saunak Dutta. SARAH and CalcHEP files with some plots are generated by Anirban Karan. The paper writing is mainly done by Priyotosh Bandyopadhyay and Anirban Karan. This project is supported by SERB CORE Grant CRG/2018/004971 and MATRICS Grant MTR/2020/000668 for the space and computing facility where Priyotosh Bandyopadhyay is the PI for the projects.

Declaration of competing interest

The authors declare that they have no known competing financial interests or personal relationships that could have appeared to influence the work reported in this paper.

Acknowledgements

PB and AK thank SERB CORE Grant CRG/2018/004971 and MATRICS Grant MTR/2020/000668 for the support. PB wants to thank Prof. Torbjörn Sjöstrand for clarification about transverse boost for the initial state in PYTHIA8.

Appendix A. Relevant functions for pair production of ϕ_v under minimal coupling

$$G_0 = 1 + \frac{1}{16}\Big[\frac{\hat{s}}{M_{\phi_v}^2} - (1+3\hat{\beta}^2)\Big]\sin^2\theta\,, \tag{A.1}$$

$$G_1 = -1 - \frac{1}{8}\Big(\frac{\hat{s}}{M_{\phi_v}^2} - 2\Big)\sin^2\theta\,, \tag{A.2}$$

$$G_3 = \frac{1}{4} + \frac{1}{16}\Big(\frac{\hat{s}}{M_{\phi_v}^2} - 2\Big)\sin^2\theta\,, \tag{A.3}$$

$$F_0 = (7+9\hat{\beta}^2\cos\theta^2)\Big[19 - 6\hat{\beta}^2 + 6\hat{\beta}^4 + (16-6\hat{\beta}^2)\,\hat{\beta}^2\cos^2\theta + 3\hat{\beta}^4\cos^4\theta\Big]\,, \tag{A.4}$$

$$F_1 = -4\Big(77 + 143\hat{\beta}^2\cos^2\theta + 36\hat{\beta}^4\cos^4\theta\Big)\,, \tag{A.5}$$

$$\begin{aligned} F_3 = {} & 2\Big(117 + 185\hat{\beta}^2\cos^2\theta + 18\hat{\beta}^4\cos^4\theta\Big) \\ & + \frac{2\,\hat{s}}{M_{\phi_v}^2}\Big(8 - \hat{\beta}^2\cos^2\theta - 7\hat{\beta}^4\cos^4\theta\Big) + \frac{7\,\hat{s}^2}{4\,M_{\phi_v}^4}\,(1-\hat{\beta}^2\cos^2\theta)^2\,, \end{aligned} \tag{A.6}$$

$$\begin{aligned} F_6 = {} & -61 - 67\hat{\beta}^2\cos^2\theta - \frac{7\,\hat{s}^2}{4\,M_{\phi_v}^4}\,(1-\hat{\beta}^2\cos^2\theta)^2 \\ & - \frac{\hat{s}}{2\,M_{\phi_v}^2}(1-\hat{\beta}^2\cos^2\theta)(39+14\hat{\beta}^2\cos^2\theta)\,, \end{aligned} \tag{A.7}$$

$$F_{10} = 3 + 5\hat{\beta}^2\cos^2\theta + \frac{5\,\hat{s}}{4\,M_{\phi_v}^2}(1-\hat{\beta}^2\cos^2\theta)(4-\hat{\beta}^2\cos^2\theta) + \frac{\hat{s}^2}{32\,M_{\phi_v}^4}(1-\hat{\beta}^2\cos^2\theta)^2(25+13\hat{\beta}^2\cos^2\theta)\,. \quad \text{(A.8)}$$

References

[1] J.L. Hewett, T.G. Rizzo, Phys. Rev. D 56 (1997) 5709–5724, https://doi.org/10.1103/PhysRevD.56.5709, arXiv: hep-ph/9703337 [hep-ph].
[2] P.A. Zyla, et al., Particle Data Group, Prog. Theor. Exp. Phys. 2020 (2020) 083C01.
[3] I. Doršner, S. Fajfer, A. Greljo, J.F. Kamenik, N. Košnik, Phys. Rep. 641 (2016) 1–68, https://doi.org/10.1016/j.physrep.2016.06.001, arXiv:1603.04993 [hep-ph].
[4] J.C. Pati, A. Salam, Phys. Rev. D 8 (1973) 1240–1251, https://doi.org/10.1103/PhysRevD.8.1240.
[5] J.C. Pati, A. Salam, Phys. Rev. D 10 (1974) 275–289, https://doi.org/10.1103/PhysRevD.10.275, erratum: Phys. Rev. D 11 (1975) 703.
[6] H. Georgi, AIP Conf. Proc. 23 (1975) 575–582, https://doi.org/10.1063/1.2947450.
[7] H. Georgi, S.L. Glashow, Phys. Rev. Lett. 32 (1974) 438–441, https://doi.org/10.1103/PhysRevLett.32.438.
[8] S. Dimopoulos, L. Susskind, https://doi.org/10.1016/0550-3213(79)90364-X.
[9] E. Farhi, L. Susskind, Phys. Rep. 74 (1981) 277, https://doi.org/10.1016/0370-1573(81)90173-3.
[10] B. Schrempp, F. Schrempp, Phys. Lett. B 153 (1985) 101–107, https://doi.org/10.1016/0370-2693(85)91450-9.
[11] J. Wudka, Phys. Lett. B 167 (1986) 337–342, https://doi.org/10.1016/0370-2693(86)90356-4.
[12] H.P. Nilles, Phys. Rep. 110 (1984) 1–162, https://doi.org/10.1016/0370-1573(84)90008-5.
[13] H.E. Haber, G.L. Kane, Phys. Rep. 117 (1985) 75–263, https://doi.org/10.1016/0370-1573(85)90051-1.
[14] A. Crivellin, D. Müller, L. Schnell, arXiv:2101.07811 [hep-ph].
[15] K. Azizi, A.T. Olgun, Z. Tavukoğlu, Chin. Phys. C 45 (1) (2021) 013113, https://doi.org/10.1088/1674-1137/abc242.
[16] G. Faisel, J.Y. Su, J. Tandean, arXiv:2012.15847 [hep-ph].
[17] G. Azuelos, O. Fischer, S. Jana, arXiv:2012.11514 [hep-ph].
[18] C. Hati, J. Kriewald, J. Orloff, A.M. Teixeira, arXiv:2012.05883 [hep-ph].
[19] S. Iguro, M. Takeuchi, R. Watanabe, arXiv:2011.02486 [hep-ph].
[20] A. Crivellin, C. Greub, D. Müller, F. Saturnino, arXiv:2010.06593 [hep-ph].
[21] M. Bordone, O. Cata, T. Feldmann, R. Mandal, arXiv:2010.03297 [hep-ph].
[22] K.S. Babu, P.S.B. Dev, S. Jana, A. Thapa, arXiv:2009.01771 [hep-ph].
[23] S. Kumbhakar, R. Mohanta, arXiv:2008.04016 [hep-ph].
[24] I. Doršner, S. Fajfer, S. Saad, Phys. Rev. D 102 (7) (2020) 075007, https://doi.org/10.1103/PhysRevD.102.075007, arXiv:2006.11624 [hep-ph].
[25] A. Crivellin, D. Müller, F. Saturnino, J. High Energy Phys. 11 (2020) 094, https://doi.org/10.1007/JHEP11(2020)094, arXiv:2006.10758 [hep-ph].
[26] P.S. Bhupal Dev, R. Mohanta, S. Patra, S. Sahoo, Phys. Rev. D 102 (9) (2020) 095012, https://doi.org/10.1103/PhysRevD.102.095012, arXiv:2004.09464 [hep-ph].
[27] I. Bigaran, R.R. Volkas, Phys. Rev. D 102 (7) (2020) 075037, https://doi.org/10.1103/PhysRevD.102.075037, arXiv:2002.12544 [hep-ph].
[28] W. Altmannshofer, S. Gori, H.H. Patel, S. Profumo, D. Tuckler, J. High Energy Phys. 05 (2020) 069, https://doi.org/10.1007/JHEP05(2020)069, arXiv:2002.01400 [hep-ph].
[29] A. Crivellin, D. Müller, F. Saturnino, J. High Energy Phys. 06 (2020) 020, https://doi.org/10.1007/JHEP06(2020)020, arXiv:1912.04224 [hep-ph].
[30] I. Doršner, S. Fajfer, O. Sumensari, J. High Energy Phys. 06 (2020) 089, https://doi.org/10.1007/JHEP06(2020)089, arXiv:1910.03877 [hep-ph].
[31] W.S. Hou, T. Modak, G.G. Wong, Eur. Phys. J. C 79 (11) (2019) 964, https://doi.org/10.1140/epjc/s10052-019-7490-0, arXiv:1909.00403 [hep-ph].
[32] R. Mandal, A. Pich, J. High Energy Phys. 12 (2019) 089, https://doi.org/10.1007/JHEP12(2019)089, arXiv:1908.11155 [hep-ph].
[33] P. Bandyopadhyay, R. Mandal, Phys. Rev. D 95 (3) (2017) 035007, https://doi.org/10.1103/PhysRevD.95.035007, arXiv:1609.03561 [hep-ph].

[34] I. Doršner, S. Fajfer, M. Patra, Eur. Phys. J. C 80 (3) (2020) 204, https://doi.org/10.1140/epjc/s10052-020-7754-8, arXiv:1906.05660 [hep-ph].
[35] S. Davidson, S. Descotes-Genon, J. High Energy Phys. 11 (2010) 073, https://doi.org/10.1007/JHEP11(2010)073, arXiv:1009.1998 [hep-ph].
[36] M. Leurer, Phys. Rev. D 49 (1994) 333–342, https://doi.org/10.1103/PhysRevD.49.333, arXiv:hep-ph/9309266 [hep-ph].
[37] N.G. Deshpande, X.G. He, S. Oh, Phys. Rev. D 51 (1995) 2295–2301, https://doi.org/10.1103/PhysRevD.51.2295, arXiv:hep-ph/9410373 [hep-ph].
[38] P. Bandyopadhyay, R. Mandal, Eur. Phys. J. C 78 (2018) 491, https://doi.org/10.1140/epjc/s10052-018-5959-x, arXiv:1801.04253 [hep-ph].
[39] K. Chandak, T. Mandal, S. Mitra, Phys. Rev. D 100 (7) (2019) 075019, https://doi.org/10.1103/PhysRevD.100.075019, arXiv:1907.11194 [hep-ph].
[40] T. Mandal, S. Mitra, S. Seth, J. High Energy Phys. 07 (2015) 028, https://doi.org/10.1007/JHEP07(2015)028, arXiv:1503.04689 [hep-ph].
[41] G. Alexander, et al., OPAL, Phys. Lett. B 263 (1991) 123–134, https://doi.org/10.1016/0370-2693(91)91717-A.
[42] M. Kramer, T. Plehn, M. Spira, P. Zerwas, Phys. Rev. Lett. 79 (1997) 341–344, https://doi.org/10.1103/PhysRevLett.79.341, arXiv:hep-ph/9704322 [hep-ph].
[43] A. Bhaskar, D. Das, T. Mandal, S. Mitra, C. Neeraj, arXiv:2101.12069 [hep-ph].
[44] U. Haisch, G. Polesello, arXiv:2012.11474 [hep-ph].
[45] L. Buonocore, U. Haisch, P. Nason, F. Tramontano, G. Zanderighi, Phys. Rev. Lett. 125 (23) (2020) 231804, https://doi.org/10.1103/PhysRevLett.125.231804, arXiv:2005.06475 [hep-ph].
[46] A. Bhaskar, T. Mandal, S. Mitra, Phys. Rev. D 101 (11) (2020) 115015, https://doi.org/10.1103/PhysRevD.101.115015, arXiv:2004.01096 [hep-ph].
[47] A. Bhaskar, D. Das, B. De, S. Mitra, Phys. Rev. D 102 (3) (2020) 035002, https://doi.org/10.1103/PhysRevD.102.035002, arXiv:2002.12571 [hep-ph].
[48] C. Borschensky, B. Fuks, A. Kulesza, D. Schwartländer, Phys. Rev. D 101 (11) (2020) 115017, https://doi.org/10.1103/PhysRevD.101.115017, arXiv:2002.08971 [hep-ph].
[49] B.C. Allanach, T. Corbett, M. Madigan, Eur. Phys. J. C 80 (2) (2020) 170, https://doi.org/10.1140/epjc/s10052-020-7722-3, arXiv:1911.04455 [hep-ph].
[50] A. Alves, O.J.P. Eboli, G. Grilli Di Cortona, R.R. Moreira, Phys. Rev. D 99 (9) (2019) 095005, https://doi.org/10.1103/PhysRevD.99.095005, arXiv:1812.08632 [hep-ph].
[51] S. Mandal, M. Mitra, N. Sinha, Phys. Rev. D 98 (9) (2018) 095004, https://doi.org/10.1103/PhysRevD.98.095004, arXiv:1807.06455 [hep-ph].
[52] R. Padhan, S. Mandal, M. Mitra, N. Sinha, Phys. Rev. D 101 (7) (2020) 075037, https://doi.org/10.1103/PhysRevD.101.075037, arXiv:1912.07236 [hep-ph].
[53] M.J. Baker, J. Fuentes-Martín, G. Isidori, M. König, Eur. Phys. J. C 79 (4) (2019) 334, https://doi.org/10.1140/epjc/s10052-019-6853-x, arXiv:1901.10480 [hep-ph].
[54] J. Blumlein, E. Boos, A. Kryukov, Z. Phys. C 76 (1997) 137–153, https://doi.org/10.1007/s002880050538, arXiv:hep-ph/9610408 [hep-ph].
[55] P. Abreu, et al., DELPHI, Phys. Lett. B 446 (1999) 62–74, https://doi.org/10.1016/S0370-2693(98)01525-1, arXiv:hep-ex/9903072 [hep-ex].
[56] S. Chekanov, et al., ZEUS, Phys. Rev. D 68 (2003) 052004, https://doi.org/10.1103/PhysRevD.68.052004, arXiv:hep-ex/0304008 [hep-ex].
[57] J. Alitti, et al., UA2, Phys. Lett. B 274 (1992) 507–512, https://doi.org/10.1016/0370-2693(92)92024-B.
[58] F. Abe, et al., CDF, Phys. Rev. Lett. 75 (1995) 1012–1016, https://doi.org/10.1103/PhysRevLett.75.1012.
[59] F. Abe, et al., CDF, Phys. Rev. Lett. 78 (1997) 2906–2911, https://doi.org/10.1103/PhysRevLett.78.2906.
[60] P. Bandyopadhyay, S. Dutta, A. Karan, arXiv:2012.13644 [hep-ph].
[61] P. Bandyopadhyay, S. Dutta, A. Karan, Eur. Phys. J. C 80 (6) (2020) 573, https://doi.org/10.1140/epjc/s10052-020-8083-7, arXiv:2003.11751 [hep-ph].
[62] M. Aaboud, et al., ATLAS, J. High Energy Phys. 06 (2019) 144, https://doi.org/10.1007/JHEP06(2019)144, arXiv:1902.08103 [hep-ex].
[63] M. Aaboud, et al., ATLAS, Eur. Phys. J. C 79 (9) (2019) 733, https://doi.org/10.1140/epjc/s10052-019-7181-x, arXiv:1902.00377 [hep-ex].
[64] A.M. Sirunyan, et al., CMS, Phys. Rev. D 99 (5) (2019) 052002, https://doi.org/10.1103/PhysRevD.99.052002, arXiv:1811.01197 [hep-ex].
[65] A.M. Sirunyan, et al., CMS, Phys. Rev. D 99 (3) (2019) 032014, https://doi.org/10.1103/PhysRevD.99.032014, arXiv:1808.05082 [hep-ex].

[66] A.M. Sirunyan, et al., CMS, Phys. Rev. D 98 (3) (2018) 032005, https://doi.org/10.1103/PhysRevD.98.032005, arXiv:1805.10228 [hep-ex].
[67] A.M. Sirunyan, et al., CMS, Eur. Phys. J. C 78 (2018) 707, https://doi.org/10.1140/epjc/s10052-018-6143-z, arXiv:1803.02864 [hep-ex].
[68] A.M. Sirunyan, et al., CMS, J. High Energy Phys. 03 (2019) 170, https://doi.org/10.1007/JHEP03(2019)170, arXiv:1811.00806 [hep-ex].
[69] W. Buchmuller, R. Ruckl, D. Wyler, Phys. Lett. B 191 (1987) 442–448, https://doi.org/10.1016/0370-2693(87)90637-X, erratum: Phys. Lett. B 448 (1999) 320.
[70] J.L. Hewett, S. Pakvasa, Phys. Rev. D 37 (1988) 3165, https://doi.org/10.1103/PhysRevD.37.3165.
[71] A. Belyaev, C. Leroy, R. Mehdiyev, A. Pukhov, J. High Energy Phys. 09 (2005) 005, https://doi.org/10.1088/1126-6708/2005/09/005, arXiv:hep-ph/0502067 [hep-ph].
[72] S. Davidson, D.C. Bailey, B.A. Campbell, Z. Phys. C 61 (1994) 613–644, https://doi.org/10.1007/BF01552629, arXiv:hep-ph/9309310 [hep-ph].
[73] M. Leurer, Phys. Rev. D 50 (1994) 536–541, https://doi.org/10.1103/PhysRevD.50.536, arXiv:hep-ph/9312341 [hep-ph].
[74] M. Carpentier, S. Davidson, Eur. Phys. J. C 70 (2010) 1071–1090, https://doi.org/10.1140/epjc/s10052-010-1482-4, arXiv:1008.0280 [hep-ph].
[75] G. Bhattacharyya, J.R. Ellis, K. Sridhar, Phys. Lett. B 336 (1994) 100–106, https://doi.org/10.1016/0370-2693(94)00927-9, erratum: Phys. Lett. B 338 (1994) 522–523, arXiv:hep-ph/9406354 [hep-ph].
[76] J.L. Hewett, T.G. Rizzo, Phys. Rev. D 36 (1987) 3367, https://doi.org/10.1103/PhysRevD.36.3367.
[77] T. Plehn, H. Spiesberger, M. Spira, P.M. Zerwas, Z. Phys. C 74 (1997) 611–614, https://doi.org/10.1007/s002880050426, arXiv:hep-ph/9703433 [hep-ph].
[78] M. Kramer, T. Plehn, M. Spira, P.M. Zerwas, Phys. Rev. Lett. 79 (1997) 341–344, https://doi.org/10.1103/PhysRevLett.79.341, arXiv:hep-ph/9704322 [hep-ph].
[79] F. Cuypers, Nucl. Phys. B 474 (1996) 57–71, https://doi.org/10.1016/0550-3213(96)00270-2, arXiv:hep-ph/9508397 [hep-ph].
[80] O.J. Eboli, E.M. Gregores, M.B. Magro, P.G. Mercadante, S.F. Novaes, Phys. Lett. B 311 (1993) 147–152, https://doi.org/10.1016/0370-2693(93)90547-U, arXiv:hep-ph/9306229 [hep-ph].
[81] H. Nadeau, D. London, Phys. Rev. D 47 (1993) 3742–3749, https://doi.org/10.1103/PhysRevD.47.3742, arXiv:hep-ph/9303238 [hep-ph].
[82] S. Atag, O. Cakir, Phys. Rev. D 49 (1994) 5769–5772, https://doi.org/10.1103/PhysRevD.49.5769.
[83] J.F. Gunion, E. Ma, Phys. Lett. B 195 (1987) 257–264, https://doi.org/10.1016/0370-2693(87)91205-6.
[84] V.A. Ilyin, A.E. Pukhov, V.I. Savrin, A.V. Semenov, W.B. von Schlippe, Phys. Lett. B 351 (1995) 504–509, https://doi.org/10.1016/0370-2693(95)00444-P, erratum: Phys. Lett. B 352 (1995) 500, arXiv:hep-ph/9503401 [hep-ph].
[85] S. Atag, A. Celikel, S. Sultansoy, Phys. Lett. B 326 (1994) 185–189, https://doi.org/10.1016/0370-2693(94)91212-2.
[86] J. Blumlein, E. Boos, A. Pukhov, Mod. Phys. Lett. A 9 (1994) 3007–3022, https://doi.org/10.1142/S0217732394002847, arXiv:hep-ph/9404321 [hep-ph].
[87] H.J. Behrend, et al., CELLO, Phys. Lett. B 178 (1986) 452–456, https://doi.org/10.1016/0370-2693(86)91410-3.
[88] W. Bartel, et al., JADE, Z. Phys. C 36 (1987) 15, https://doi.org/10.1007/BF01556160.
[89] G.N. Kim, et al., AMY, Phys. Lett. B 240 (1990) 243–249, https://doi.org/10.1016/0370-2693(90)90442-9.
[90] D. Decamp, et al., ALEPH, Phys. Rep. 216 (1992) 253–340, https://doi.org/10.1016/0370-1573(92)90177-2.
[91] O. Adriani, et al., L3, Phys. Rep. 236 (1993) 1–146, https://doi.org/10.1016/0370-1573(93)90027-B.
[92] G. Abbiendi, et al., OPAL, Eur. Phys. J. C 31 (2003) 281–305, https://doi.org/10.1140/epjc/s2003-01325-y, arXiv:hep-ex/0305053 [hep-ex].
[93] H. Abramowicz, et al., ZEUS, Phys. Rev. D 86 (2012) 012005, https://doi.org/10.1103/PhysRevD.86.012005, arXiv:1205.5179 [hep-ex].
[94] H. Abramowicz, et al., ZEUS, Phys. Rev. D 99 (9) (2019) 092006, https://doi.org/10.1103/PhysRevD.99.092006, arXiv:1902.03048 [hep-ex].
[95] F.D. Aaron, et al., H1, Phys. Lett. B 704 (2011) 388–396, https://doi.org/10.1016/j.physletb.2011.09.017, arXiv:1107.3716 [hep-ex].
[96] D. Acosta, et al., CDF, Phys. Rev. D 72 (2005) 051107, https://doi.org/10.1103/PhysRevD.72.051107, arXiv:hep-ex/0506074 [hep-ex].
[97] A. Abulencia, et al., CDF, Phys. Rev. D 73 (2006) 051102, https://doi.org/10.1103/PhysRevD.73.051102, arXiv:hep-ex/0512055 [hep-ex].
[98] T. Aaltonen, et al., CDF, Phys. Rev. D 77 (2008) 091105, https://doi.org/10.1103/PhysRevD.77.091105, arXiv:0706.2832 [hep-ex].

[99] V.M. Abazov, et al., D0, Phys. Lett. B 671 (2009) 224–232, https://doi.org/10.1016/j.physletb.2008.12.017, arXiv:0808.4023 [hep-ex].
[100] V.M. Abazov, et al., D0, Phys. Lett. B 693 (2010) 95–101, https://doi.org/10.1016/j.physletb.2010.08.028, arXiv:1005.2222 [hep-ex].
[101] V.M. Abazov, et al., D0, Phys. Rev. D 84 (2011) 071104, https://doi.org/10.1103/PhysRevD.84.071104, arXiv:1107.1849 [hep-ex].
[102] T. Sjöstrand, S. Ask, J.R. Christiansen, R. Corke, N. Desai, P. Ilten, S. Mrenna, S. Prestel, C.O. Rasmussen, P.Z. Skands, Comput. Phys. Commun. 191 (2015) 159–177, https://doi.org/10.1016/j.cpc.2015.01.024, arXiv:1410.3012 [hep-ph].
[103] F. Staub, Comput. Phys. Commun. 185 (2014) 1773–1790, https://doi.org/10.1016/j.cpc.2014.02.018, arXiv:1309.7223 [hep-ph].
[104] A. Belyaev, N.D. Christensen, A. Pukhov, Comput. Phys. Commun. 184 (2013) 1729–1769, https://doi.org/10.1016/j.cpc.2013.01.014, arXiv:1207.6082 [hep-ph].
[105] M. Cacciari, G.P. Salam, G. Soyez, Eur. Phys. J. C 72 (2012) 1896, https://doi.org/10.1140/epjc/s10052-012-1896-2, arXiv:1111.6097 [hep-ph].
[106] E.R. Nocera, et al., NNPDF, Nucl. Phys. B 887 (2014) 276–308, https://doi.org/10.1016/j.nuclphysb.2014.08.008, arXiv:1406.5539 [hep-ph].
[107] D. Krohn, M.D. Schwartz, T. Lin, W.J. Waalewijn, Phys. Rev. Lett. 110 (21) (2013) 212001, https://doi.org/10.1103/PhysRevLett.110.212001, arXiv:1209.2421 [hep-ph].
[108] S. Tokar, ATLAS, CMS, ATL-PHYS-PROC-2017-017.
[109] A.M. Sirunyan, et al., CMS, J. High Energy Phys. 10 (2017) 131, https://doi.org/10.1007/JHEP10(2017)131, arXiv:1706.05868 [hep-ex].
[110] G. Aad, et al., ATLAS, J. High Energy Phys. 10 (2020) 112, https://doi.org/10.1007/JHEP10(2020)112, arXiv:2006.05872 [hep-ex].
[111] A.M. Sirunyan, et al., CMS, Phys. Lett. B 819 (2021) 136446, https://doi.org/10.1016/j.physletb.2021.136446, arXiv:2012.04178 [hep-ex].